*Human Molecular Genetics*, 2019, Vol. 28, No. 4 598–614

**doi: 10.1093/hmg/ddy371**
Advance Access Publication Date: 17 October 2018
General Article

GENERAL ARTICLE

# A recurrent missense variant in *SLC9A7* causes nonsyndromic X-linked intellectual disability with alteration of Golgi acidification and aberrant glycosylation

Wujood Khayat[1], Anna Hackett[2], Marie Shaw[3], Alina Ilie[1], Tracy Dudding-Byth[2], Vera M. Kalscheuer[4], Louise Christie[2], Mark A. Corbett[3], Jane Juusola[5], Kathryn L. Friend[6], Brian M. Kirmse[7], Jozef Gecz[3,8,†], Michael Field[2,*] and John Orlowski[1,*]

[1]Department of Physiology, McGill University, Montreal, Quebec H3G 0B1, Canada, [2]Genetics of Learning Disability Service, Hunter Genetics, Waratah, NSW 2298, Australia, [3]Adelaide Medical School and Robinson Research Institute, The University of Adelaide, Adelaide, SA 5000, Australia, [4]Research Group Development and Disease, Max Planck Institute for Molecular Genetics, D-14195 Berlin, Germany, [5]GeneDx, Gaithersburg, MD 20877, USA, [6]Genetics and Molecular Pathology, SA Pathology, Adelaide, SA 5006, Australia, [7]Department of Pediatrics, Division of Medical Genetics, University of Mississippi Medical Center, Jackson, MS 39216, USA and [8]South Australian Health and Medical Research Institute, Adelaide, SA 5000, Australia

*To whom correspondence should be addressed at: Department of Physiology, McGill University, Bellini Life Sciences Bldg., Rm, 166, 3649 Promenade Sir-William-Osler Montreal, Quebec H3G 0B1, Canada. Tel: +1 5143988335; Email: john.orlowski@mcgill.ca; Genetics of Learning Disability Service, Hunter Genetics, Waratah, NSW 2298, Australia. Tel: +61 0294631551; Email: mike.field@health.nsw.gov.au

## Abstract

We report two unrelated families with multigenerational nonsyndromic intellectual disability (ID) segregating with a recurrent *de novo* missense variant (c.1543C>T:p.Leu515Phe) in the alkali cation/proton exchanger gene *SLC9A7* (also commonly referred to as *NHE7*). *SLC9A7* is located on human X chromosome at Xp11.3 and has not yet been associated with a human phenotype. The gene is widely transcribed, but especially abundant in brain, skeletal muscle and various secretory tissues. Within cells, SLC9A7 resides in the Golgi apparatus, with prominent enrichment in the *trans*-Golgi network (TGN) and post-Golgi vesicles. In transfected Chinese hamster ovary AP-1 cells, the Leu515Phe mutant protein was correctly targeted to the TGN/post-Golgi vesicles, but its *N*-linked oligosaccharide maturation as well as that of a co-transfected secretory membrane glycoprotein, vesicular stomatitis virus G (VSVG) glycoprotein, was reduced compared to cells co-expressing SLC9A7 wild-type and VSVG. This correlated with alkalinization of the TGN/post-Golgi compartments, suggestive of a gain-of-function. Membrane trafficking of glycosylation-deficient Leu515Phe and co-transfected VSVG to the cell surface, however, was relatively unaffected. Mass spectrometry analysis of patient sera also revealed an abnormal

[†]Jozef Gecz, http://orcid.org/0000-0002-7884-6861
**Received:** June 28, 2018. **Revised:** October 10, 2018. **Accepted:** October 12, 2018

N-glycosylation profile for transferrin, a clinical diagnostic marker for congenital disorders of glycosylation. These data implicate a crucial role for SLC9A7 in the regulation of TGN/post-Golgi pH homeostasis and glycosylation of exported cargo, which may underlie the cellular pathophysiology and neurodevelopmental deficits associated with this particular nonsyndromic form of X-linked ID.

## Introduction

Syndromic and nonsyndromic forms of intellectual disability (ID) affect ~1–2% of the human population and are characterized by pronounced limitations in both cognitive capabilities and adaptive behaviours covering various social and practical life skills (1,2). The underlying etiologies are diverse and complex, ranging from external influences (e.g. birth complications, malnutrition, infectious agents, substance abuse) to genetic perturbations (e.g. chromosomal abnormalities, epigenetic dysregulation, single-gene mutations), with the latter accounting for at least half of reported cases. The advent of next generation DNA sequencing approaches has greatly accelerated the pace of discovery of *de novo* mutations in known as well as in novel candidate genes associated with idiopathic ID (3–5). To date, over 700 genes are linked to monogenic forms of ID (6), with a disproportionate fraction (i.e. >100 genes) located on the X-chromosome (7–11). These genes cover the gamut of biological processes, ranging from events in the nucleus such as genome replication, chromatin remodelling and transcription to extra-nuclear activities involving signal transduction, cytoskeletal dynamics, metabolism, vesicular trafficking, glycosylation and membrane excitability (12–19). It is not unexpected that mutations that impact on these critical cellular functions can profoundly affect central nervous system development and cognitive functioning (20,21).

In the present study, we describe a novel recurrent missense variant (NM_001257291.1:c.1543C>T:p.Leu515Phe) in the *SLC9A7* gene (solute carrier family 9, member A7, also commonly called *NHE7*; OMIM 300368) located at chromosome position Xp11.3, which gives rise to a nonsyndromic form of ID, characterized by moderate to severe cognitive dysfunction, with brisk reflexes, hypotonia, muscle weakness and bilateral clinodactyly. *SLC9A7* is widely transcribed with prominent expression in brain, skeletal muscle and various secretory tissues, including reproductive organs, adrenal, gastric, pancreas, pituitary, thyroid, salivary and mammary glands and encodes an alkali cation ($Na^+$, $K^+$)/proton ($H^+$) exchanger that resides in the Golgi, with preferential accumulation in the *trans*-Golgi network (TGN) and post-Golgi vesicles (22) (also, see human RNAseq expression data at https://www.ncbi.nlm.nih.gov/gene/84679 and https://www.gtexportal.org/home/gene/SLC9A7). We investigate the effects of this mutation on the biosynthetic processing, stability and membrane trafficking of SLC9A7 and its impact on Golgi function.

## Results

### Clinical features and genetic analysis

We recently identified four males in an Australian (AU) family who presented with moderate to severe ID, significant speech delay, reserved personality, early hypotonia, muscle weakness, variable deep tendon reflexes, and bilateral clinodactyly (Fig. 1A; for additional description of the family history, see Supplementary Material). Females were clinically unaffected. Because of the male bias, X chromosome haplotype analysis was performed with 5 cM polymorphic markers in seven informative males (including the four males with ID and three unaffected male relatives). A shared haplotype was observed in all affected males between markers DXS8080 and DXS1196 covering a region of 41.8 Mbp between Xp11.3 and Xq21.1. The multipoint linkage data gave a logarithmic odds score of 1.49 (23). The haplotypes in IV:2 and IV:5 indicated the disease-causing variant was on the paternally inherited allele in IV:2 assuming X-linked inheritance. As III:1 was reported to be of normal intelligence, any pathogenic variant was assumed to have occurred as a *de novo* mutation in IV:2. Using X-exome sequencing (11) of proband VI:1, we identified one variant of unknown significance in *SLC9A7* (NM_001257291.1:c.1543C>T:p.Leu515Phe) located at chromosome position Xp11.3, a locus suggested to be enriched for genes linked to neurogenetic disorders (24). This variant would be present in all expressed splice transcripts of *SLC9A7* (SLC9A7v1: 726 amino acids, NCBI NM_001257291.1; SLC9A7v2, 725 amino acids, NCBI NM_032591.2; http://www.ncbi.nlm.nih.gov/).

Sanger sequencing confirmed the missense variant in VI:1, and subsequent segregation analysis showed that this variant was present in all affected males and also in IV:2. The variant was absent in IV:5, a sister of IV:2 who inherited the same X chromosome from their father. As IV:5 was negative for the variant, this suggested that the variant arose *de novo* on the paternal allele [i.e. their father's (III:1) X chromosome] of IV:2. In order to confirm this was the only novel coding or non-coding variant within this haplotype not shared by III:1 and the four affected males, we performed whole-genome sequencing of the affected male VI:1 and of IV:5, the putative non-carrier daughter of III:2. We extracted low-frequency hemizygous sequence variants present in VI:1 but not in IV:5, assuming a quality score for that base call of >60 in both samples. Of 23 906 hemizygous variant calls in this region in VI:1, the only unique variant reaching these thresholds was the previously identified c.1543C>T:p.Leu515Phe variant in *SLC9A7*. The presence of small copy number variations below the resolution of conventional cytogenetic array was examined using Lumpy (a probabilistic framework for discovering structural variants) (25), with no variants overlapping coding genes identified in this region.

Case matching through colleagues and the Matchmaker Exchange portal (https://www.matchmakerexchange.org/) (26) identified a second family in the United States of America (family US) with the same variant in the proband IV:2 and his maternal uncle III:5 who presented with a similar phenotype including early hypotonia and gross motor delay, whilst the uncle was semi-independent as an adult (Fig. 1B; for clinical and family history, see Supplementary Material). The older photographs of males in both families (Fig. 1) show some similarities including a high anterior hairline, long face with a fine nose, deep nasolabial folds and slightly downturned angles of the mouth. Extraction of variant reads within 100 kb proximal and distal of *SLC9A7* in both families showed that the variant was not present on a common haplotype and that these two families were unrelated (*data not shown*).

Amino acid Leu515 in SLC9A7 is highly conserved evolutionarily at the analogous positions of other human SLC9A isoforms (tolerating only isoleucine as a substitution) and is invariant

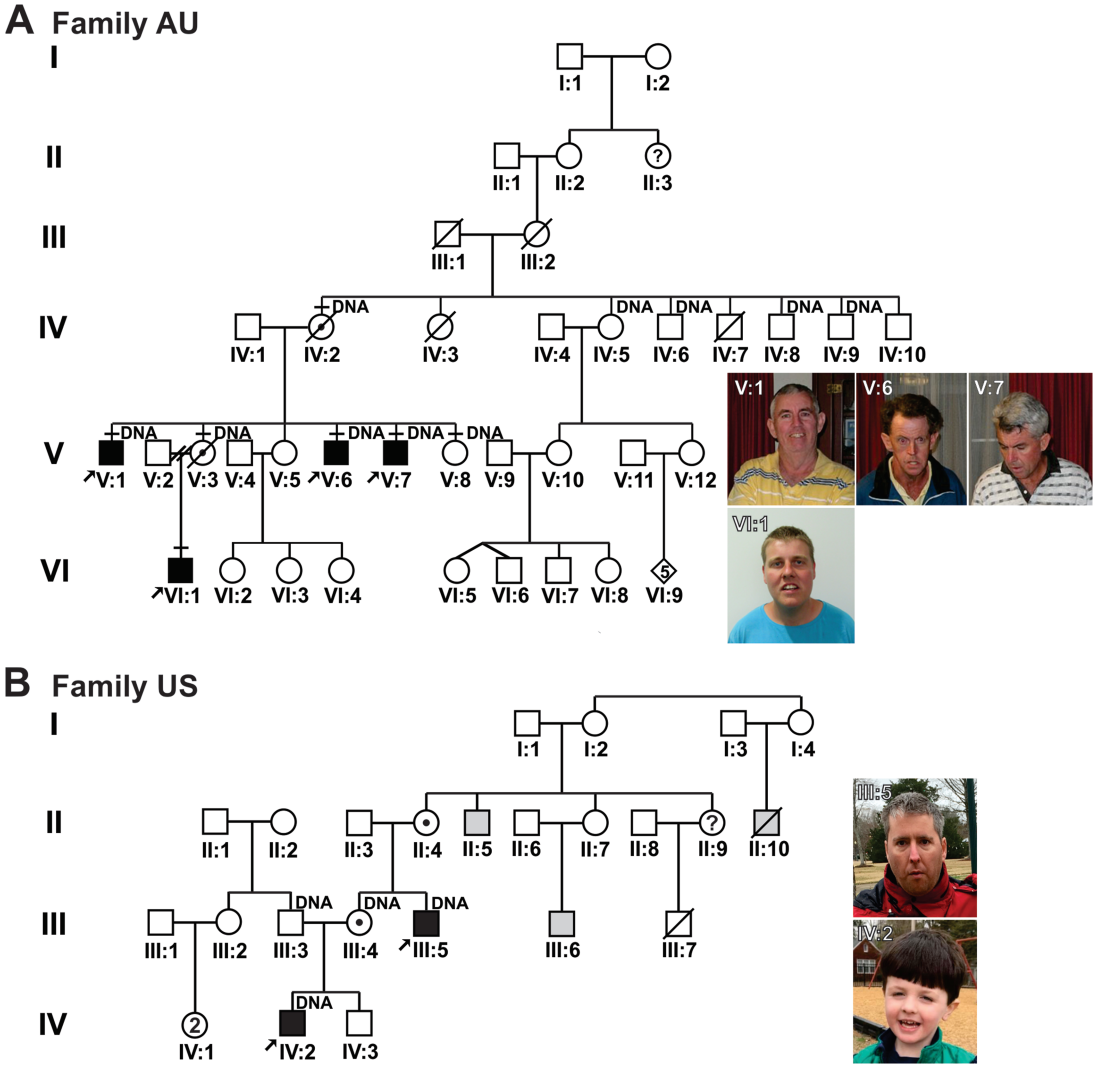


**Figure 1.** Pedigree of two families affected by a recurrent missense variation in *SLC9A7*. (**A**), Pedigree of family AU with four affected males at the fifth and sixth generations (*shaded in black*) who are confirmed carriers of the p.Leu515Phe variant in SLC9A7. Pictures show individuals V:1, V:6, V:7 and VI:1 aged 65, 58, 56 and 27 years, respectively. (**B**) Pedigree of family US and pictures of two affected males at the third (III:5; age, 36 years) and fourth (IV:2; age, 4 years) generations (*shaded in black*) carrying the same p.Leu515Phe variant in SLC9A7. Carrier females are indicated by circles with a dot. Other male members of family US (II:5, II:10 and III:6) (*shaded in gray*) were diagnosed with developmental disabilities without a confirmed/known genetic etiology. Genetic analyses indicated that the common mutation is on distinct alleles, indicating that the families are unrelated.

in SLC9A7 orthologues from chimpanzees to zebrafish (Fig. 2), suggesting that leucine at this position might be crucial for transporter structure and/or function. This observation is further supported by the fact that this region of the protein has a low residual variation intolerance score as measured by the missense tolerance ratio calculator (27) (Supplementary Material, Fig. S1). In keeping with this, the variant is absent in the gnomAD population control database (http://gnomad.broadinstitute.org/gene/ENSG00000065923) (28).

## Assessment of the biosynthesis, post-translational maturation and stability of SLC9A7

To evaluate the effects of the p.Leu515Phe (L515F) mutation on SLC9A7 function, the substitution was introduced into the cDNA of wild-type (WT) SLC9A7v1 that also contained an influenza virus hemagglutinin (HA) epitope at its C-terminus (simply referred to as $WT_{HA}$ and $L515F_{HA}$) for high-affinity immunological detection. For certain experiments, the SLC9A7 constructs were also fused at their C-terminus to mCherry fluorescent protein (i.e. $WT_{ChFP}$ and $L515F_{ChFP}$). The tagged WT and L515F constructs were then expressed in a subline of Chinese hamster ovary cells (AP-1 cells) to measure and compare their molecular and cellular properties, including the rates of biosynthesis and post-translational maturation, protein half-life, subcellular localization, Golgi pH homeostasis and function. This cell line was chosen for study because the level of endogenous SLC9A7 protein in AP-1 cells is very low or negligible, as revealed by western blotting and immunocytochemistry of AP-1 cells using an isoform-specific rabbit polyclonal antibody against SLC9A7 developed in our laboratory (Supplementary Material, Fig. S2). Hence, this cell line serves as an amenable model system to compare the properties of exogenous WT and L515F without the confounding presence of endogenous SLC9A7 protein.

SLC9A7, like other SLC9A isoforms, assembles as a homodimer and is purportedly glycosylated at a single N-glycosylation

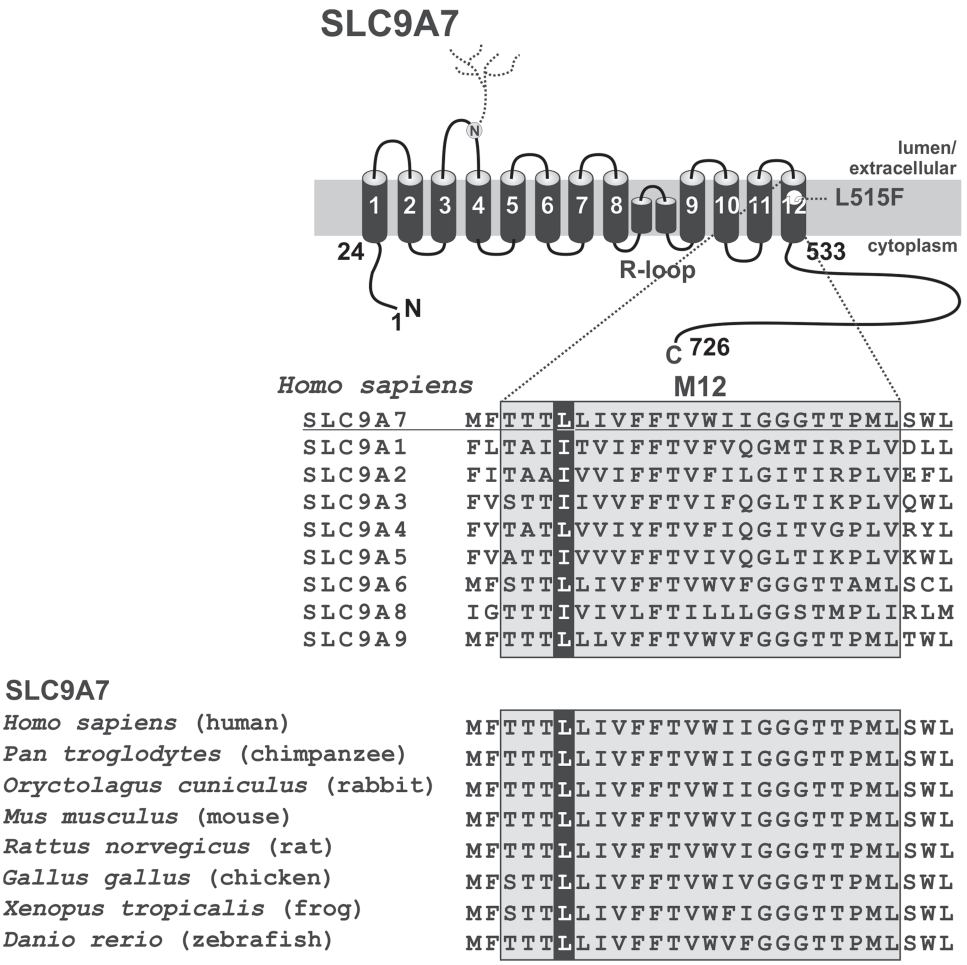


**Figure 2.** Membrane topology and missense variant (p.Leu515Phe) in human *SLC9A7*. The *upper panel* is a schematic illustration of the predicted membrane topology of human SLC9A7v1 and the location where leucine is substituted for phenylalanine at position 515 in the predicted twelfth membrane-spanning helix (M12) of SLC9A7. The *middle* and *lower panels* are sequence alignments of amino acids in M12 of human SLC9A isoforms and orthologous proteins from different species, respectively, showing that Leu515 is highly conserved across phylogeny.

site ($^{145}$NVS) in its predicted second extracellular loop (22). To evaluate the biosynthetic maturation of SLC9A7, AP-1 cells were transiently transfected with $WT_{HA}$ or $L515F_{HA}$ over a 72 h period. As presented in Figure 3A, $WT_{HA}$ typically migrates as multiple bands in sodium dodecyl sulfate polyacrylamide gel electrophoresis (SDS-PAGE) gels reflecting the oligomeric and glycosylated states of the protein, a pattern that mimics other SLC9A isoforms (29–31) (also see Supplementary Material, Fig. S2A). The two highest molecular weight bands represent: (1) mature hybrid/complex glycoconjugates or fully-glycosylated (*fg*, ~270 kDa) (i.e. Golgi processed) and (2) immature high-mannose or core-glycosylated (*cg*, ~250 kDa) [i.e. endoplasmic reticulum (ER) processed] dimeric forms of SLC9A7 that do not fully dissociate under SDS-PAGE conditions. The faster migrating, lower molecular weight bands represent the dissociated fully glycosylated (*fg*) and core-glycosylated (*cg*) monomeric forms of SLC9A7, though in some lanes the nascent unglycosylated (*ug*) protein is partially discernable (see Fig. 3A, second lane showing $L515F_{HA}$ at 6 h). Compared to $WT_{HA}$, $L515F_{HA}$ showed reduced levels of protein expression and oligosaccharide maturation, with a larger fraction of the protein accumulating as immature core-glycosylated dimeric and monomeric species. As a control for protein loading, the membranes were stripped and reblotted against the ER resident protein, calnexin. To compare the relative degrees of glycosylation of the $WT_{HA}$ and $L515F_{HA}$ proteins, the signal intensities of the bands at an intermediate time point (24 h post-transfection) were quantified by densitometry of X-ray films exposed in the linear range and analysed using ImageJ software. The analyses indicated that the level of glycosylation (expressed as % glycosylated bands *per* total SLC9A7 protein level) of $WT_{HA}$ was 5-fold higher than $L515F_{HA}$ (Fig. 3B). These results indicate that post-translational processing of $L515F_{HA}$ along the biosynthetic pathway is partially impaired compared to its $WT_{HA}$ counterpart.

To confirm the general nature of the oligosaccharide modifications of SLC9A7, AP-1 cells were transiently transfected with $WT_{HA}$ or $L515F_{HA}$ for 36 h, lysed in non-detergent buffers and post-nuclear supernatants were untreated or treated with either endoglycosidase H (Endo H), which cleaves only simpler asparagine-linked (*N*-linked) mannose-rich carbohydrate chains (i.e. core-glycosylated) but not more intricate fully glycosylated oligosaccharides, or peptide-*N*-glycosidase F (PNGase F), which removes all *N*-linked oligosaccharide structures. As shown in the immunoblots presented in Figure 3C, Endo H treatment reduced the size of only the core-glycosylated $WT_{HA}$ and $L515F_{HA}$ proteins, although the cleavage was incomplete under the recommended reaction conditions. In contrast, PNGase F

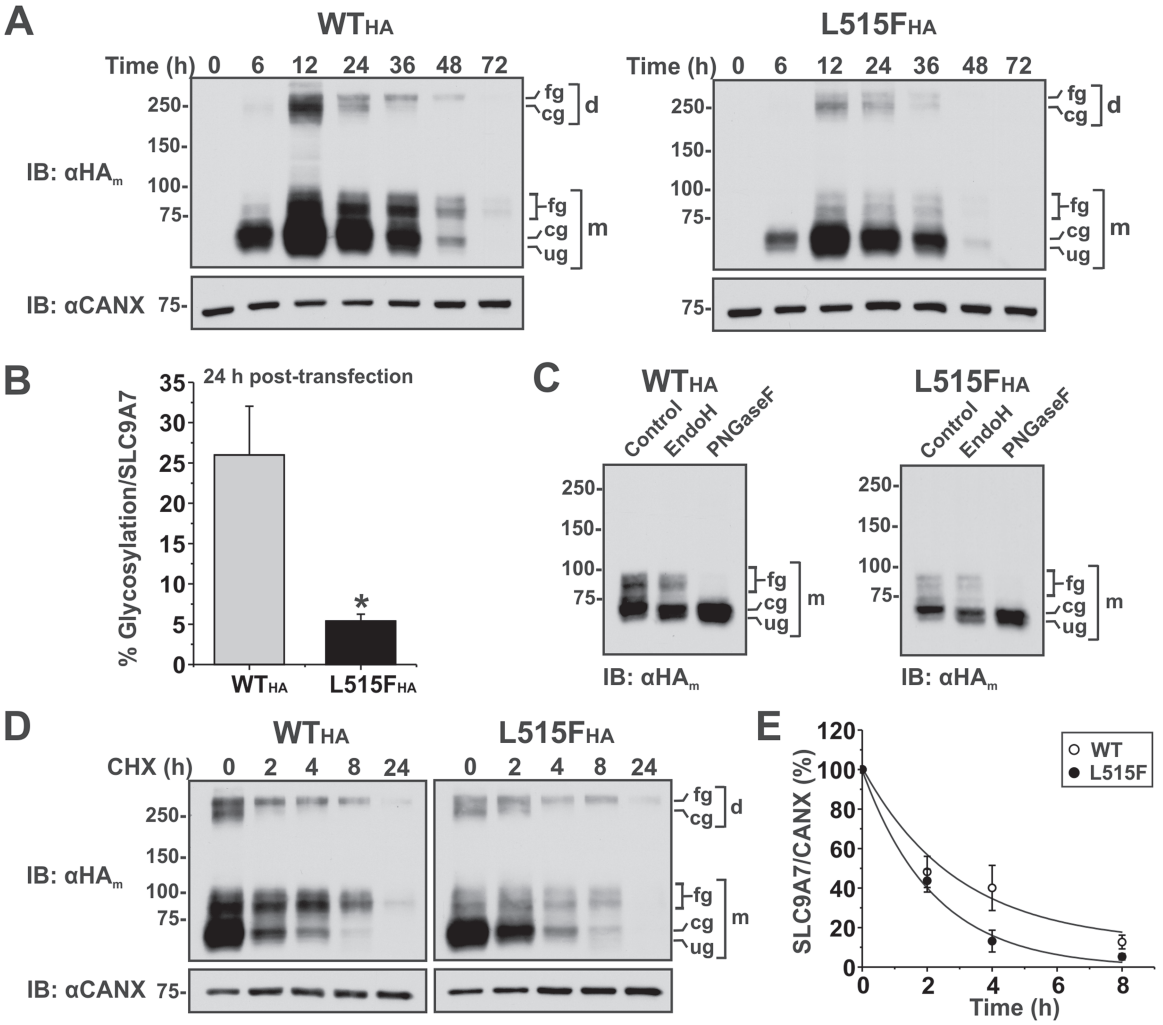


**Figure 3.** Assessment of the oligosaccharide maturation and stability of SLC9A7 WT and L515F mutant in transiently transfected Chinese hamster ovary AP-1 cells. (**A**) AP-1 cells were transiently transfected with $SLC9A7_{HA}$ WT or L515F mutant and lysed at the indicated time points over a 72 h period. Equal amounts of proteins were subjected to SDS-PAGE and immunoblotting with a monoclonal anti-HA antibody ($\alpha HA_m$). SLC9A7 migrates as multiple bands: slower migrating high molecular weight bands representing the fully-glycosylated (*fg*, ~270 kDa) and core-glycosylated (*cg*, ~250 kDa) dimeric forms of the exchanger that do not fully dissociate under SDS-PAGE conditions and faster migrating fully-glycosylated (*fg*, ~80–100 kDa), core-glycosylated (*cg*, ~70 kDa) and unglycosylated (*ug*, ~68 kDa) forms of the monomeric protein. The same blots were also probed with a polyclonal $\alpha$CANX as a loading control. (**B**) The signal intensities of the fully glycosylated bands relative to the total protein levels of WT and L515F at an intermediate time point (24 h post-transfection) were quantified by densitometry of X-ray films exposed in the linear range and analysed using ImageJ software. Values represent the mean ± S.E.M. ($n = 7$). Asterisks; two-sample Student's *t*-test; $P < 0.01$. (**C**) AP-1 cells transiently expressing $SLC9A7_{HA}$ WT or L515F were lysed in non-detergent buffer 36 h post-transfection. Post-nuclear supernatants were left untreated (control) or treated with *N*-glycosidase enzymes, Endo H or PNGase F. The western blots are representative of 3–4 experiments. (**D**) AP-1 cells were transiently transfected with $SLC9A7_{HA}$ WT or L515F for 24 h and then treated with cycloheximide (150 µg/ml) for the indicated time points to inhibit *de novo* protein synthesis. Cells were then lysed and equal amounts of proteins were subjected to SDS-PAGE and immunoblotting using a mouse monoclonal anti-HA ($\alpha HA_m$) antibody to detect $SLC9A7_{HA}$ and an antibody to calnexin ($\alpha$CANX) as a loading control. (**E**) Quantitative analysis by densitometry of $WT_{HA}$ and $L515F_{HA}$ protein abundance (normalized to calnexin levels) as a function of time in the presence of cycloheximide. Data were modelled to an exponential decay using the fit function ($y = A1^{*}\exp(-x/t1) + y0$). The adjusted R-squared ($R^2$) values for $WT_{HA}$ and $L515F_{HA}$ are 0.917 and 0.986, respectively. The half-life ($t_{1/2}$) of $L515F_{HA}$ was slightly reduced compared to $WT_{HA}$ (2.2 ± 0.43 h versus 2.92 ± 1.52 h, respectively), though the difference was not statistically significant ($P > 0.05$, one-way ANOVA with a Tukey *post-hoc* test). Values represent the mean ± S.E.M. of six separate experiments.

removed all the *N*-linked oligosaccharide structures resulting in unglycosylated, faster migrating forms of SLC9A7. It was noted that the bands representing the dimeric forms of SLC9A7 were not evident in these blots, most likely due to their complete dissociation under the buffers conditions used for the glycosidase treatments.

As mentioned above, the biosynthesis data presented in Figure 3A show that the level of $L515F_{HA}$ protein expression is slightly reduced compared to $WT_{HA}$. To determine whether the mutation affected the half-life of the transporter, a pulse-chase experiment was carried out. AP-1 cells were transiently transfected with the SLC9A7 constructs for 24 h and then treated with cycloheximide to block new protein synthesis over a subsequent 24 h period. Cellular lysates were obtained at the indicated time points after cycloheximide treatment and analysed by western blotting and densitometry to monitor residual protein levels as a function of time. As shown in Figure 3D and E, both $WT_{HA}$ and $L515F_{HA}$ transporters exhibited rapid turnover rates, with the half-life ($t_{1/2}$) of $L515F_{HA}$ being slightly reduced compared to $WT_{HA}$, though this difference did not reach statistical significance (L515F: 2.2 ± 0.43 h *versus* WT: 2.92 ± 1.52 h, $P > 0.05$).

### Subcellular localization of SLC9A7

Previous studies (22,32,33) have shown that SLC9A7 localizes to the Golgi apparatus, with preferential accumulation in the TGN and post-Golgi vesicles and a minor fraction at the cell surface as it transients along the secretory pathway. We postulated that the observed reduction in post-translational processing and maturation of L515F could be due to impaired protein trafficking from the ER to the Golgi. To examine this possibility, AP-1 cells were transiently co-transfected with a TGN-specific marker, TGN46 tagged at its cytoplasmic-oriented C-terminus with emerald green fluorescent protein (GFP) ($TGN46_{EmGFP}$) and SLC9A7 WT or L515F fused at their C-terminus to mCherry fluorescent protein ($WT_{ChFP}$ and $L515F_{ChFP}$, respectively). The fluorescent cell images revealed that both $WT_{ChFP}$ and $L515F_{ChFP}$ were properly targeted to the TGN and post-Golgi vesicles as indicated by the high degree of signal overlap with $TGN46_{EmGFP}$ (Supplementary Material, Fig. S3A).

To determine whether the mutation altered surface expression of SLC9A7, we utilized a cell surface biotinylation assay (34) to selectively extract plasma membrane (PM) proteins of AP-1 cells transiently expressing $WT_{HA}$ or $L515F_{HA}$ at 24 and 48 h post-transfection. As shown in the immunoblots presented in Supplementary Material, Figure S3B, both fully and core-glycosylated $WT_{HA}$ and $L515F_{HA}$ were able to traffic to the cell surface at both time points. For the $WT_{HA}$ transporter, there was an enrichment of the fully glycosylated relative to the core-glycosylated species at the cell surface, whereas this ratio was reversed for the mutant $L515F_{HA}$. Based on densitometric quantification of the signal intensities of SLC9A7 and the relative levels of protein in the total cell lysates (TCLs) and PM fractions, the amount of $WT_{HA}$ at the cell surface was estimated to be ~3% of its total cellular expression at 24 h post-transfection. The normalized proportion of $L515F_{HA}$ transporters at the cell surface relative to its total cellular expression level was slightly reduced compared to $WT_{HA}$ at both time points (Supplementary Material, Fig. S3C), but the differences were not statistically significant (two-sample Student's *t*-test, $P > 0.05$). This indicates that the mutation did not markedly alter the delivery of $L515F_{HA}$ to the PM.

### Ratiometric measurement of pH in SLC9A7-containing endomembrane compartments

Progressive acidification of organelles along the biosynthetic pathway is known to be important for post-translational processing (e.g. glycan maturation, pre-prohormone cleavage), sorting and transport of nascent proteins (35,36). Earlier studies have established that the luminal pH of the ER is near neutrality and mirrors that of the cytoplasm (~pH 7.1–7.2) (37,38), but becomes progressively more acidic within the Golgi cisternae (~pH 6.4–6.6) (38–40), TGN (~pH 6.0–6.4) (41–44) and secretory vesicles (pH 5.2–5.7) (43,45). Active accumulation of $H^+$ in organelles of the secretory pathway is achieved by the electrogenic vacuolar-type $H^+$-ATPase (46,47) and is accompanied by parallel movements of counterions such as $Cl^-$ through various anion channels (48–51) that neutralize the buildup of positive charge that would otherwise decrease $H^+$-ATPase activity. In addition, $H^+$ efflux pathways exist to counterbalance $H^+$-ATPase-driven acidification in order to achieve an optimal acidic pH environment, though the precise mechanisms have yet to be fully resolved. Earlier studies described a $Zn^{2+}$-inhibitable, voltage-sensitive $H^+$ conductance in the Golgi complex (52), but its molecular identity remains obscure. SLC9A7 (22) and SLC9A8 (53,54) have also been proposed as potential routes for electroneutral $H^+$ efflux in exchange for cytoplasmic $K^+$ (or $Na^+$) in the Golgi and post-Golgi compartments. In support of this notion, overexpression of SLC9A8 in COS7 cells resulted in alkalinization of the mid- to trans-cisternae of the Golgi complex using a pH-sensitive probe targeted to those compartments (53). However, a role for SLC9A7 in pH regulation of the Golgi has yet to be demonstrated empirically.

To selectively measure the intraluminal pH of only SLC9A7-containing endomembrane compartments, we inserted the cDNA for the ratiometric pH-sensitive GFP variant pHluorin2 (pH2) (55) in-frame within the first extracellular loop of WT and L515F ($_{pH2}$WT and $_{pH2}$L515F), which would orient the fluorophore into the endomembrane lumen (illustrated in Fig. 4A). This insertion did not appear to alter the biosynthesis or the subcellular distribution of either chimeric construct compared to their respective parental transporters in transiently transfected AP-1 cells (Fig. 4B, and *data not shown*). The endomembrane pH ($pH_e$) of these compartments was measured using a fluorescence ratiometric image analysis (FRIA) technique (56). For our $pH_e$ measurements, a laser-scanning confocal microscope was used to illuminate the cells alternately with 405 and 488 nm light and the emitted fluorescence was detected between 500 and 550 nm. To standardize the fluorescence ratio values (R488/405) as a function of $pH_e$, calibration curves were performed *in situ* in AP-1 cells expressing $_{pH2}$WT by clamping the intraluminal $pH_e$ between 5.0 and 7.8 in $K^+$-rich medium containing bafilomycin, an inhibitor of the vacuolar $H^+$-ATPase and ionophores to equilibrate pH across membrane compartments and the extracellular solution. For each pH level, ~25–50 vesicles or endomembrane clusters per cell were imaged and the average R488/405 values were calculated. The collected data were used to generate the calibration curve presented in Figure 4C. To compare the intraluminal $pH_e$ profiles of $_{pH2}$WT and $_{pH2}$L515F-containing endomembrane compartments, AP-1 cells were transiently transfected with each construct for 24 h and then incubated with cycloheximide for an additional 3 h to block new protein synthesis while allowing the existing $_{pH2}$WT and $_{pH2}$L515F to mature biosynthetically and accumulate in the TGN and post-Golgi vesicles prior to measuring $pH_e$ (Fig. 4B). During imaging, cells were maintained under physiological culture conditions in a microscope stage-top thermostatted incubation chamber [i.e. complete alpha-minimum essential medium ($\alpha$-MEM) media buffered with 22 mM $NaHCO_3$ and equilibrated with 5% $CO_2$ and 95% air at 37°C]. The distribution of $_{pH2}$WT and $_{pH2}$L515F-containing compartments (aggregate endomembrane pool from 15 cells) as a function of their $pH_e$ is presented in Figure 4D, with the median $pH_e$ value for $_{pH2}$L515F compartments shifted noticeably to more alkaline values compared to $_{pH2}$WT (median $pH_e$ 6.49 ± 0.02 versus 6.17 ± 0.03, respectively). Calculation of the mean steady state $pH_e$ of $_{pH2}$WT-containing endomembrane compartments per cell was 6.07 ± 0.03 ($n = 31$) cells] (Fig. 4E), a value within the range of those previously documented for the TGN (pH 6.0–6.4) (41,42,44). In contrast, the mean $pH_e$ of $_{pH2}$L515F-containing endomembranes was significantly more alkaline, i.e. $pH_e$ 6.57 ± 0.04 ($n = 31$, $P < 0.001$, two-sample Student's *t*-test).

Despite concordance with previous measurements of TGN $pH_e$, insertion of pH2 into the first extracellular loop of SLC9A7 might have affected its catalytic properties, thereby distorting estimates of TGN $pH_e$. Another potential shortcoming to using the $_{pH2}$SLC9A7 constructs as pH sensors is that TGN $pH_e$ cannot be assessed independently of exogenous SLC9A7

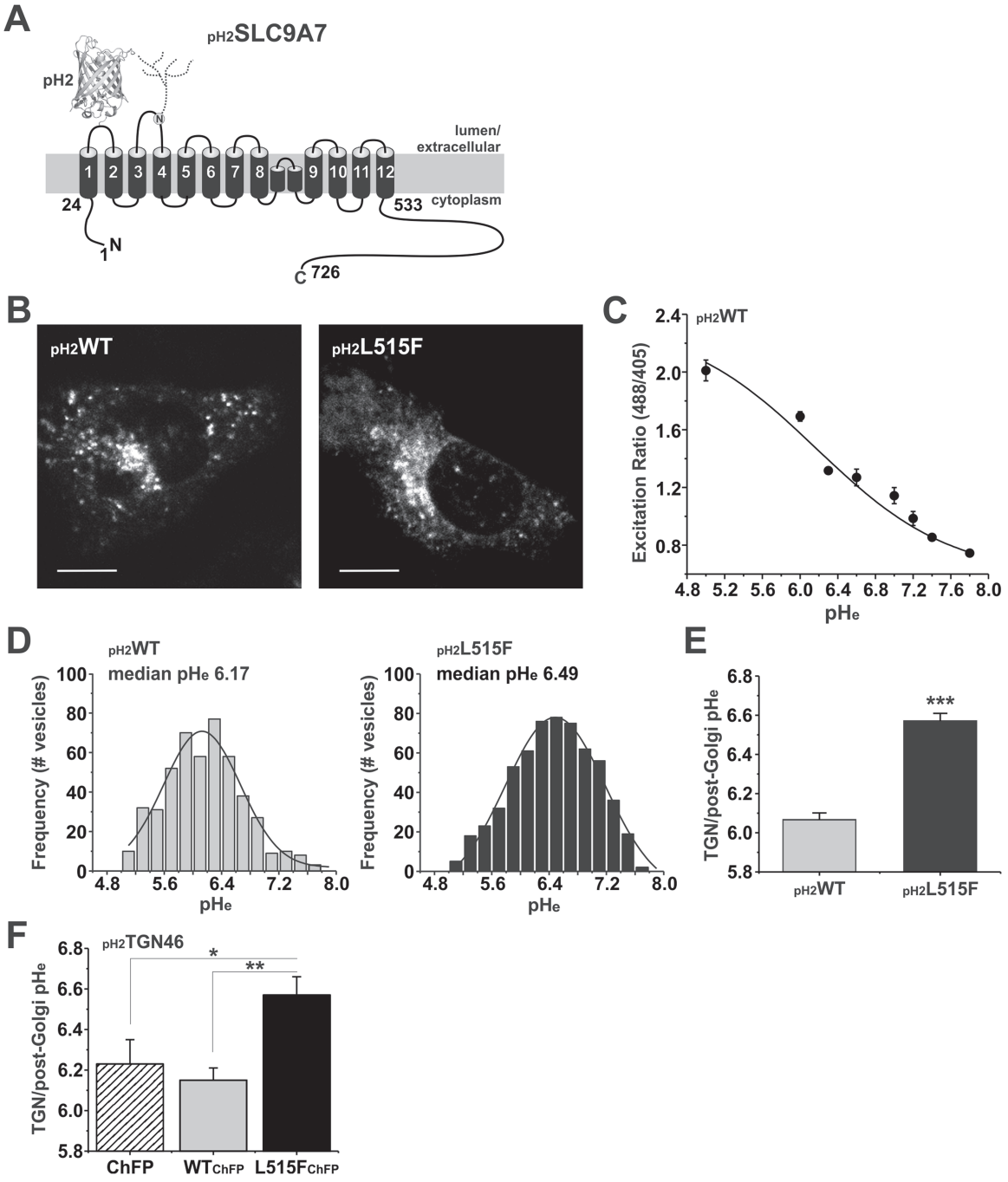


**Figure 4.** Acidification of SLC9A7 L515F-containing endomembrane compartments is impaired. (**A**) Illustration of SLC9A7 containing the pH-sensitive GFP fluorophore pHluorin2 (pH2) inserted into its first extracellular loop ($_{pH2}$SLC9A7). (**B**) Representative fluorescence images of AP-1 cells expressing $_{pH2}$WT or $_{pH2}$L515F. Scale bar, 10 µm. (**C**) The panel shows the in situ calibration curve of pH2 fluorescence (excitation ratio 488/405) inserted in $_{pH2}$WT as a function of endomembrane pH ($pH_e$) performed by clamping intracellular pH between 5 and 7.8, as described in 'Material and Methods'. (**D**) Frequency distribution of $_{pH2}$WT- and $_{pH2}$L515F-endomembrane compartments/vesicles (combined from 15 cells) as a function of their intraluminal $pH_e$. (**E**) Plot of the average intraluminal $pH_e$ of $_{pH2}$WT- and $_{pH2}$L515F-containing endomembrane compartments per cell (mean ± S.E.M., $n = 31$ cells). Asterisks; two-sample Student's *t*-test, $P < 0.001$. (**F**) Plot of the average TGN $pH_e$ in AP-1 cells transiently co-expressing (24 h) the pH-sensitive probe $_{pH2}$TGN46 and ChFP, $WT_{ChFP}$ or $L515F_{ChFP}$ (mean ± S.E.M., $n = 6$–8 cells). Asterisks; $^*P < 0.05$; $^{**}P < 0.01$ (one-way ANOVA with a Tukey *post-hoc* test).

expression. To address these considerations, we constructed a separate TGN-specific pH-sensitive probe by fusing pH2 into the luminal-facing N-terminal domain of TGN46 ($_{pH2}$TGN46). In transfected AP-1 cells, the signals of the $_{pH2}$TGN46 probe accumulated in a juxtanuclear compartment that overlapped those of $WT_{ChFP}$ and $L515F_{ChFP}$ (Supplementary Material, Fig. S4A) and responded appropriately to experimentally induced changes in intracellular pH (Supplementary Material, Fig. S4B), thereby confirming the subcellular localization and fidelity of the TGN pH-sensing probe. TGN pH was then assessed in AP-1 cells co-transfected with $_{pH2}$TGN46 and ChFP, $WT_{ChFP}$ or $L515F_{ChFP}$ following the same experimental conditions used for the

$_{pH2}$SLC9A7 probes. As shown in Figure 4F, the TGN $pH_e$ of cells separately expressing $WT_{ChFP}$ and $L515F_{ChFP}$ was 6.15 ± 0.06 and 6.58 ± 0.09, respectively, and corroborate our previous $pH_e$ measurements with $_{pH2}$WT and $_{pH2}$L515F (i.e. pH 6.07 ± 0.03 and 6.57 ± 0.04, respectively). Collectively, these results suggest that the exchange activity of the mutant L515F is altered, possibly enhanced, though the precise nature of the catalytic dysfunction remains to be determined. Curiously, and unexpectedly, there was no significant difference in resting TGN $pH_e$ of AP-1 cells which lack SLC9A7 expression ($pH_e$ 6.23 ± 0.12) compared to the $WT_{ChFP}$-transfectants ($pH_e$ 6.15 ± 0.06). Because at steady state the rates of the $H^+$ pump and leak are identical, the finding that overexpression of WT SLC9A7 did not induce alkalization [i.e. cytoplasmic $K^+$ (or $Na^+$) influx in exchange for luminal $H^+$ efflux] above resting levels suggests that, at least in AP-1 cells, the rates of acidification mediated by endogenous vacuolar $H^+$-ATPases and counterion conductances are not limiting and are sufficient to counter the additional $H^+$ efflux mediated by the exogenous WT exchanger, but are inadequate in the presence of the 'hyperactive' L515F mutant. However, further studies would be required to elucidate the precise underlying mechanism.

### VSVG glycosylation and membrane trafficking

As mentioned above, the acidic environment of the Golgi is recognized as an important determinant of protein and lipid glycosylation and trafficking, as well as maintenance of Golgi morphology (51,57–60). Given the observed impairment in glycosylation of the L515F mutant, we sought to determine whether other glycoproteins might be similarly affected when co-expressed with L515F. To this end, we performed a pulse-chase experiment utilizing a temperature-sensitive variant (ts045) of the vesicular stomatitis virus G (VSVG) glycoprotein that was tagged with GFP ($VSVG_{GFP}$) (61,62). This glycoprotein variant misfolds and is retained in the ER when cells are incubated at 40°C; however, upon shifting the temperature to 32°C, the protein refolds to its proper conformation and is transported synchronously out of the ER to the Golgi and post-Golgi compartments. To monitor both glycosylation and cell surface trafficking of $VSVG_{GFP}$, AP-1 cells were transiently transfected with $VSVG_{GFP}$ alone or in the presence of either $WT_{HA}$ or $L515F_{HA}$ at 37°C. At 24 h post-transfection, some cell cultures were treated with the membrane-impermeable reagent *N*-hydroxysulfosuccinimydyl-SS-biotin to label PM proteins and lysed to examine $VSVG_{GFP}$ protein levels in the total lysates and cell surface fractions (control), whereas the remainder of the cell cultures were shifted to 40°C in order to accumulate $VSVG_{GFP}$ in the ER. Next, cells in other culture dishes were biotinylated and lysed after 20 h of incubation at 40°C, whereas the remainder were shifted to 32°C for the indicated time points after being treated with cycloheximide (100 µg/ml) to prevent additional protein synthesis while allowing for synchronous export of the existing proteins from the ER to the Golgi and PM. As shown in the immunoblots presented in Figure 5A, shifting the temperature to 40°C resulted in $VSVG_{GFP}$ remaining largely in its faster-migrating core-glycosylated state under all transfection conditions. At the permissive temperature of 32°C, $VSVG_{GFP}$ was progressively glycosylated to its mature form in the absence or presence of $WT_{HA}$. In contrast, addition of more complex *N*-glycans to $VSVG_{GFP}$ did not occur in cells co-expressing $L515F_{HA}$. However, there were no apparent differences in cell surface delivery of $VSVG_{GFP}$ under each experimental condition, irrespective of it state of glycosylation, which peaked between 60 and 120 min and decreased thereafter (Fig. 5B). These data suggest that $L515F_{HA}$ expression impaired $VSVG_{GFP}$ glycosylation, but had minimal effect on its trafficking to the PM.

To validate the importance of acidification on complex glycosylation of $VSVG_{GFP}$, we repeated the experimental protocol described above by co-transfecting $VSVG_{GFP}$ with $WT_{HA}$ in the absence or presence of 50 nM bafilomycin, a potent inhibitor of the vacuolar $H^+$-ATPase that causes rapid alkalinization (within 10–20 min) of the Golgi as well as other acidic endomembrane compartments (42,44). As presented in Figure 5C, bafilomycin treatment prevented glycosylation of $VSVG_{GFP}$ in the presence of $WT_{HA,}$ a result similar to that obtained in untreated cells co-expressing L515F (shown in Fig. 5A). As expected, $pH_e$ within the TGN/post-Golgi compartments rapidly alkalinized in the presence of bafilomycin using SLC9A7 $_{pH2}$WT as a pH-sensitive probe in companion cultures (Fig. 5D). Collectively, these results indicate that proper acidification of the Golgi is critical for complex glycosylation of SLC9A7 as well as other secretory cargo.

To assess whether these *in vitro* findings have clinical relevance, we measured the *N*-glycosylation profile of serum transferrin in affected males of both families AU and US. This is a widely used clinical diagnostic assay to screen for *N*-linked congenital disorders of glycosylation (63–66). Normal transferrin contains two complex-type *N*-glycan sites, each comprised of a disialylated biantennary oligosaccharide chain, as the dominant species (i.e. the tetra-sialo form) and minor forms containing fucosylated or triantennary glycans (63). Biochemical measurement of serum transferrin by capillary electrophoresis in three of the affected males in family AU failed to demonstrate any abnormality. However, in family US using a more sensitive affinity chromatography–mass spectrometry method (Mayo Clinical Laboratories, Rochester, Minnesota, USA, comparable assay not available in Australia) (67), we detected an abnormally high ratio of the tri-sialo/di-oligosaccharide chain that was most significant in affected male IV:2 (Table 1), suggesting absence of a single sialic acid moiety.

## Discussion

In this study, we identified and evaluated a novel recurrent missense variant (c.1543C>T, p.Leu515Phe) in the ($Na^+$, $K^+$)/$H^+$ exchanger gene *SLC9A7* in two multigenerational Australian and American families with four and two affected males, respectively, who displayed moderate to severe ID that correlates with prominent expression of SLC9A7 mRNA in brain. This is the first report of a disease-causing variation in *SLC9A7* and adds to a growing list of neurodevelopmental disorders associated with other SLC9A family members, including Lichtenstein–Knorr syndrome (*SLC9A1*) (68), Christianson syndrome (*SLC9A6*) (69,70), autism spectrum disorder (*SLC9A6* and *SLC9A9*) (71,72) and attention deficit hyperactivity disorder (*SLC9A9*) (73–75).

Previous studies (22,32,33) have shown that SLC9A7 is sorted to the Golgi, with preferential accumulation in the TGN and post-Golgi vesicles that shuttle secretory cargo to the PM. In transfected Chinese hamster ovary AP-1 cells, we found that the L515F mutation did not significantly affect the transporter's protein stability or membrane trafficking. However, while the protein half-lives of WT and L515F were comparable (2.92 ± 1.52 h versus 2.2 ± 0.43 h, respectively), their turnover rates were rapid compared to the longevity ($t_{1/2}$ > 24 h) of the closely related recycling endosomal SLC9A6 isoform (~68% identity) when overexpressed in the same cell line (76). While speculative, the short half-life of SLC9A7 suggests that it may be preferentially targeted for degradation after its delivery to the PM rather than returned to the TGN, at least when expressed exogenously in this cell

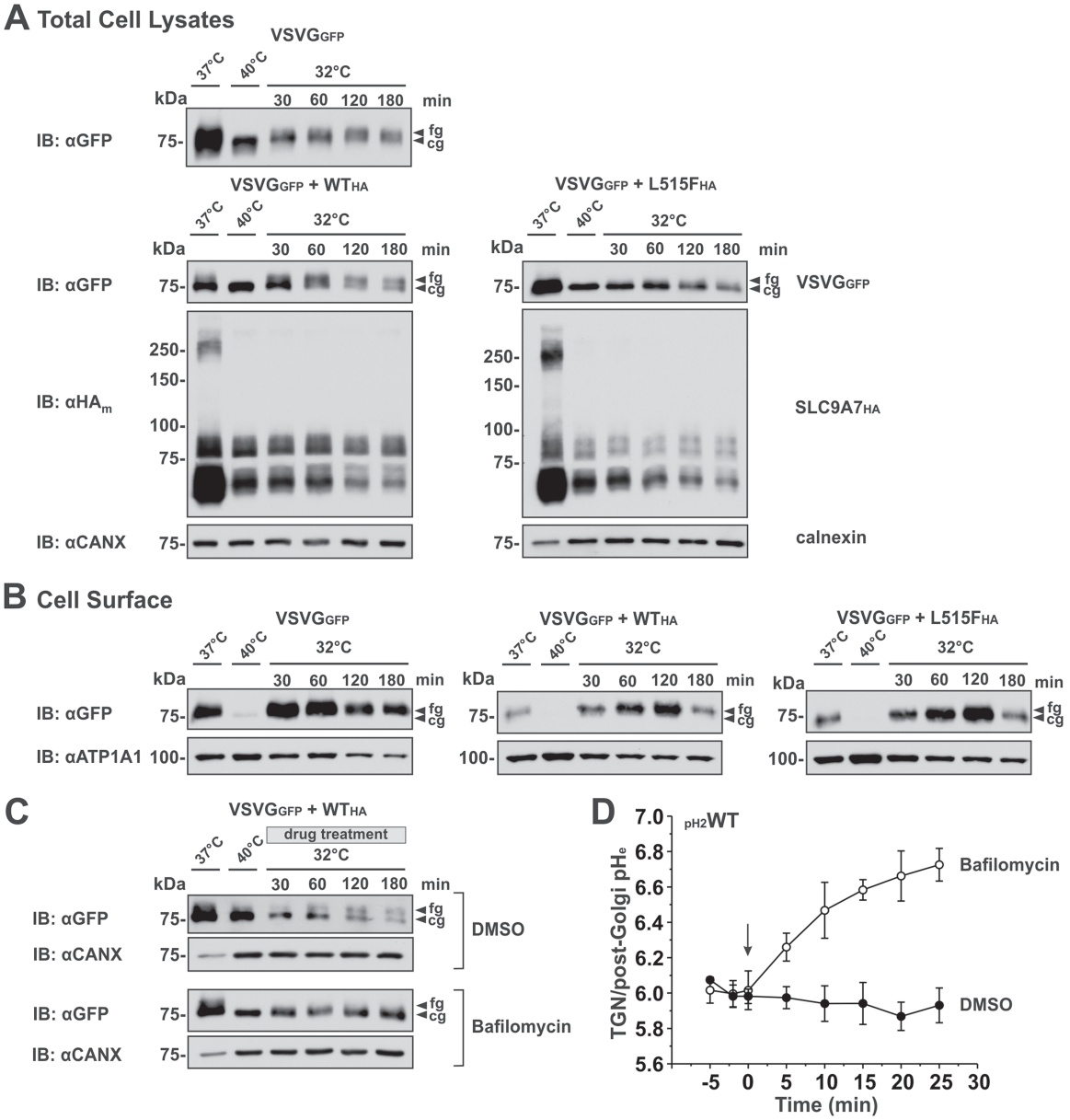


**Figure 5.** $VSVG_{GFP}$ glycosylation but not membrane trafficking is impaired in AP-1 cells expressing SLC9A7-L515F. AP-1 cells were transiently transfected with a temperature-sensitive variant of the viral glycoprotein VSVG tagged with GFP ($VSVG_{GFP}$) either alone or together with $SLC9A7_{HA}$ WT or L515F ($WT_{HA}$ or $L515F_{HA}$) for 24 h at 37°C. The temporal trafficking and oligosaccharide maturation of $VSVG_{GFP}$ along the biosynthetic pathway can be controlled in a temperature-sensitive manner. Shifting the temperature from 37–40°C for 20 h causes the protein to accumulate in the ER. A subsequent temperature shift to 32°C allows $VSVG_{GFP}$ to exit the ER and traffic along the secretory pathway (Golgi and PM). Cells were also treated with cycloheximide (100 μg/ml) to block further protein synthesis. TCL (**A**) and PM proteins isolated using a cell surface biotinylation protocol (**B**) were prepared at the indicated times and then subjected to SDS-PAGE and immunoblotting using a polyclonal GFP antibody (αGFP) to examine $VSVG_{GFP}$ glycosylation (*cg*, core-glycosylated; *fg*, fully glycosylated) or a mouse monoclonal anti-HA antibody (αHA) to detect $SLC9A7_{HA}$. For loading controls, calnexin (CANX) and $Na^+/K^+$-ATPase (ATP1A1) expression were measured as markers for TCL and PM fraction, respectively. Blots are representative of three independent experiments. (**C**) AP-1 cells were transiently co-transfected with $VSVG_{GFP}$ and $WT_{HA}$ and incubated as described above. Upon shifting the temperature to 32°C, cells were treated with cycloheximide (100 μg/ml) and DMSO (control) or vacuolar $H^+$-ATPase inhibitor bafilomycin (50 nM). Lysates were collected at the indicated time points and evaluated by SDS-PAGE and immunoblotting with αGFP. (**D**) Quantification of intraluminal $pH_e$ of the TGN/post-Golgi vesicles measured in AP-1 cells expressing $_{pH2}$WT and treated with bafilomycin. The *arrow* indicates time of addition of bafilomycin. Values are mean ± S.E.M. of three separate experiments, each performed in duplicate.

line. This is unlike certain other TGN-associated membrane proteins such as TGN38/TGN46 (77,78) or furin (79–81), which constitutively recycle between the TGN and PM.

While the L515F substitution had minimal effects on SLC9A7 stability and sorting, the extent of N-linked complex glycosylation of the transporter was noticeably reduced. Likewise, addition of N-linked glycans to an exogenously expressed secretory cargo protein, VSVG glycoprotein, was largely abolished in cells expressing L515F compared to WT. These changes correlated with alkalinization of the TGN and associate compartments where SLC9A7 is expressed (i.e. $pH_e$: L515F, 6.58 ± 0.09 versus WT, 6.15 ± 0.06). Curiously, overexpression of WT did not elevate the resting TGN $pH_e$ (i.e. $pH_e$ 6.23 ± 0.12) in native AP-1 cells lacking endogenous SLC9A7. The reason for this is unclear. We speculate

**Table 1.** Glycosylation profile of plasma transferrin in family US using affinity chromatography–mass spectrometry

| Transferrin: N-glycosylation | Reference range | Patient III:5 | Patient IV:5 |
|---|---|---|---|
| Mono-oligo/Di-oligo ratio: | ≤ 0.06 | 0.05 | 0.05 |
| Asialo-oligo/Di-oligo ratio: | ≤ 0.011 | 0.010 | 0.003 |
| Trisialo-oligo/Di-oligo ratio: | ≤ 0.05 | 0.06* | 0.12** |

Asterisks indicate values outside the normal range, with values for the proband IV:5 being the most pronounced.

that since at steady state pH, the rates of the $H^+$ pump and leak are identical, $H^+$ pumping by the vacuolar $H^+$-ATPase must have sufficient capacity to counter the additional $H^+$ efflux mediated by the exogenous WT exchanger, but was unable to sustain this level of acidification in the presence of the L515F mutant. This finding could be explained by enhanced ($Na^+$, $K^+$)/$H^+$ exchange of the L515F variant, i.e. an effect compatible with a gain-of-function. Alternatively, the mutation might have perturbed the structural integrity of its ion permeation pathway, resulting in uncoupled $H^+$ leakage through the transporter. Irrespective of the exact mechanism, a consequence of L515F expression is reduced acidification of the TGN. Our data provide the first indication of a potential regulatory role for SLC9A7 in Golgi pH homeostasis and merits further investigation. Our results also indicate that native AP-1 cells are capable of acidifying the TGN to optimal levels in the absence of SLC9A7, presumably through contributions from other Golgi-localized $H^+$ efflux pathways such as a $Zn^{2+}$-inhibitable voltage-sensitive $H^+$ conductance (52) and SLC9A8 (53,54), though this remains to be established. In this regard, it is interesting to note that two unrelated families presenting with an isolated X-linked retinitis pigmentosa 2 (RP2) without associated ID were identified as having a contiguous gene deletion of both *SLC9A7* and *RP2* (MIM 312600) (82), suggesting that gain, rather than loss, of SLC9A7 function is associated with ID. In the case of the individuals with X-linked RP2, the loss of SLC9A7 may have been compensated for by the other Golgi $H^+$ efflux pathways mentioned above.

The elevated TGN pH caused by the L515F variant (ΔpH ~0.5 units) is pronounced and has the potential to disrupt normal Golgi function. For instance, the spatial and temporal regulation of glycan biosynthesis within the Golgi has been found to be exquisitely sensitive to intraluminal pH levels (83,84). Subtle increases in Golgi pH by only 0.2 units are sufficient to interfere with the most pH-sensitive step in *N*-oligosaccharide maturation of proteins, the terminal α-(2,3)-sialylation, by inducing mislocalization of the α-(2,3)-sialyltransferase into endosomal compartments (85). More pronounced increases in Golgi pH cause additional mislocalization of other glycosyltransferases as well as altered Golgi morphology (83–85). As mentioned above, the diminished acidification of the TGN and associated compartments elicited by L515F impaired its own glycosylation as well as that of VSVG, but did not affect their subsequent trafficking to the cell surface. This pattern mimics earlier findings obtained with chemical agents that dissipate the $H^+$ gradient across the Golgi membrane and disrupt complex glycosylation of secretory cargo without impacting their delivery to the PM (86–89). Likewise, loss-of-function mutations in subunits of the V-ATPase (90,91) or in Golgi pH regulator (GPHR), a Golgi-resident chloride channel (51), also thwart Golgi acidification and complex glycosylation. However, in these latter instances, they were also accompanied by disorganization of Golgi morphology and delayed trafficking of secretory cargo. The basis for these overlapping but differing outcomes are unclear, but may reflect the severity of regionalized pH dysregulation within the Golgi apparatus as well as differences in the molecular and cellular context. Collectively, these data indicate that defective Golgi/TGN acidification elicited by L515F could account for the observed protein hypoglycosylation.

Measurement of abnormal carbohydrate-deficient forms of circulating serum transferrin is used clinically as a diagnostic tool to screen for congenital disorders of glycosylation (63,64). In this regard, we examined the *N*-glycosylation pathway in three of the affected males in family AU by capillary electrophoresis of the various transferrin glycoforms, but did not find any abnormality typical of a classical carbohydrate glycoprotein deficiency (*data not shown*). However, in family US, a more sensitive mass spectroscopy test demonstrated a high trisialo/di-oligosaccharide chain ratio that suggests absence of a single sialic acid moiety. The difference in investigation reflects the reduced sensitivity of the capillary electrophoresis that is unable to quantify ratios of each species but acts as a baseline screening investigation. To date, further blood collection and testing has not been possible for the AU family, but we would assume a similar pattern would be demonstrated. The hyposialylated transferrin pattern bears similarity to other type II congenital disorders of glycosylation associated with mutations in genes associated with the conserved oligomeric Golgi complex (92).

Glycosylation of proteins and lipids affects numerous cellular processes that are vital for embryonic and postnatal development (93–96). Hence, it is not unexpected that impaired *N*-glycan biosynthesis causes or contributes to the progression of various pathophysiological conditions, including cancers, muscular dystrophies, immune dysfunction and neurological disorders (66,84,97–101). In the nervous system, polysialylation is essential for normal migration and differentiation of neural precursor cells (102,103), cell–cell and cell–matrix adhesion (104,105) and synapse formation (106). Within synapses, *N*-glycosylation of synaptophysin and synaptic vesicle protein 2 is required for optimal synaptic vesicle trafficking (107,108). Likewise, *N*-glycosylation promotes protein stability, membrane trafficking and/or activity of various neurotransmitter transporters (109–114) and voltage-gated ion channels (115–121), which are crucial for membrane excitability and neurotransmission, and is necessary for cellular processes underlying learning and memory (122,123).

It should also be considered that the disease phenotype may be driven by disruption of other Golgi processes arising from defective SLC9A7 function. The activity of the TGN membrane-associated endoprotease furin, which catalyzes the cleavage of precursor proteins into their active forms, is pH-sensitive (124) and utilizes intraluminal $K^+$ as a regulatory cofactor (125). Thus, SLC9A7 may play an indirect role not only in protein glycosylation but also potentially in the processing of pro-proteins or propeptides into their active forms that could affect central nervous system function.

In conclusion, this study implicates the organellar SLC9A7 isoform in nonsyndromic X-linked ID. We postulate that this unique, recurrent nonsynonymous variant (p.Leu515Phe) acts as a gain-of-function disease-causing mutation. Mechanistic studies in transfected cells revealed that expression of the mutant SLC9A7 results in diminished acidification of the TGN and associated endomembrane compartments that impaired post-translational glycosylation processing of SLC9A7 and ectopically expressed VSVG glycoproteins and was found to

have a parallel affect *in vivo*. We postulate that optimal TGN pH and proper glycosylation of other proteins required for normal development and function of the nervous system might underlie this neuropathic phenotype. Further investigation will be required to determine the precise molecular and cellular mechanisms underlying this disorder.

## Materials and Methods

### Ethics approval and consent to participate

Genetic studies were approved by local ethics committees. Written informed consent was obtained for molecular genetic analysis and written permission was obtained before the publication of clinical data and photographs from all participants or their legal guardians.

### DNA sequencing and alignment

DNA was extracted from blood (QIAamp DNA blood maxi kit, Qiagen, Hilden, Germany). X-exome sequencing and alignment was performed in one member of family AU IV:6 (Fig. 1) as described by Hu *et al.* (11). Subsequent whole-genome sequencing and alignment was performed on IV:6 and VI:1 as previously described (126). Using genomic DNA from the proband and parents, the exonic regions and flanking splice junctions of the genome were captured using the Clinical Research Exome kit (Agilent Technologies, Santa Clara, CA). Massively parallel (NextGen) sequencing was done on an Illumina system with 100 bp or greater paired-end reads. Reads were aligned to human genome build GRCh37/UCSC hg19 and analysed for sequence variants using a custom-developed analysis tool. Additional sequencing technology and variant interpretation protocol have been previously described (127). The general assertion criteria for variant classification are publicly available on the GeneDx ClinVar submission page (http://www.ncbi.nlm.nih.gov/clinvar/submitters/26957/).

### Affinity chromatography-mass spectrometry

This test was developed and its performance characteristics determined by the Mayo Clinic Laboratories (Rochester, MN, USA) in a manner consistent with the Clinical Laboratory Improvement Amendments (https://www.cms.gov/Regulations-and-Guidance/Legislation/CLIA/index.html).

### Antibodies and reagents

Mouse monoclonal anti-HA antibody was purchased from Covance Inc. (Berkeley, CA, USA). Rabbit polyclonal anti-GFP antibody was from Life Technologies. Mouse monoclonal anti-β-tubulin was from Sigma. Rabbit polyclonal anti-calnexin antibody (αCANX) was from Enzo Life Sciences, Inc. Mouse monoclonal anti-$Na^+/K^+$-ATPase α1 antibody was purchased from Affinity BioReagents (Thermo Fisher Scientific Inc.). The Emerald GFP-tagged TGN46 ($TGN46_{EmGFP}$) was a gift from Michael Davidson (Addgene, mEmerald-TGNP-N-10 plasmid #54279). Horseradish peroxidase-conjugated secondary IgG antibodies were purchased from Jackson ImmunoResearch Laboratories (West Grove, PA, USA). α-MEM, fetal bovine serum, penicillin/streptomycin and trypsin-EDTA were purchased from Wisent (Saint-Bruno, QC, Canada). All other chemical and reagents were obtained from BioShop Canada (Burlington, ON, Canada), Sigma or Fisher Scientific and were of the highest grade available.

### Anti-SLC9A7 antibody production

To generate a polyclonal antibody specific for SLC9A7, a recombinant fusion protein of glutathione S-transferase (GST) and an isoform-specific C-terminal segment of human SLC9A7 (amino acids 551-582) was constructed by cloning into the *Bam*HI/*Eco*RI sites of the pGEX-2 T vector (Amersham Biosciences). After sequence verification, the plasmid was transformed into the Epicurean Coli BL21-Codon Plus™ strain (Stratagene, Cedar Creek, TX, USA). The GST-fusion protein was purified by incubating bacterial lysates with glutathione-Sepharose™ beads (GE Healthcare). Rabbit immunizations with the fusion protein were performed at the McGill Animal Resource Centre (Montreal, QC, Canada) using standard Canadian Council on Animal Care-approved protocols. Following collection of the rabbit serum, the polyclonal SLC9A7 antibodies were affinity purified as follows: the C-terminal region of SLC9A7 (amino acids 551-582) was fused in frame with the maltose binding protein (MBP) by cloning into the *Eco*RI/*Bam*HI sites of the pMAL-c2X vector (New England Biolabs, Mississauga, ON, Canada). The MBP-fusion protein was purified from *E.coli* BL-21 cultures by binding to 50% slurry of amylose resin (New England Biolabs, Mississauga, ON, Canada). The purified fusion protein was run on a 10% SDS-PAGE and then transferred onto a polyvinylidene difluoride membrane (Millipore, Nepean, ON, Canada) overnight. The membrane strip was then incubated with 2 ml of rabbit serum containing the SLC9A7 antibody at 4°C overnight. After extensive washes with 50 mM TRIS buffer, the antibody was eluted with 50 mM glycine pH 2.5 for 15 min, neutralized with 2 M TRIS (tris(hydroxymethyl)aminomethane) pH 8.0 and dialyzed overnight at 4°C in PBS. The antiserum was concentrated by using Amicon® Ultra centrifugal filter devices with 5 kDa cut off (Millipore), diluted with equal amounts of glycerol and stored at −20°C.

### Recombinant DNA constructs and mutagenesis

The longest splice variant (v1) of SLC9A7 was engineered to contain the influenza virus HA epitope (YPYDVPDYAS) at its extreme C-terminus to create WT $SLC9A7_{HA}$. This construct was inserted into the *Hind*III and *Xba*I sites of the mammalian expression vector pcDNA3 (Invitrogen) and then used as a template to engineer the L515F missense substitution by polymerase chain reaction (PCR) mutagenesis. A monomeric Cherry fluorescent protein (ChFP) was also fused to the C-terminus of SLC9A7 WT and L515F ($WT_{ChFP}$ and $L515F_{ChFP}$). In separate constructs, the pH-sensitive GFP pHluorin2 (pH2) (55) was inserted in the first extracellular loop (at amino acid position M54) of WT and L515F SLC9A7 ($_{pH2}$WT and $_{pH2}$L515F). Insertion of the different fluorescent protein tags in these positions did not alter the biosynthesis properties or cellular distribution of SLC9A7 compared to C-terminal HA-tagged versions of SLC9A7 (22). The pHluorin2-TGN46 ($_{pH2}$TGN46) was engineered by replacing GFP in the mammalian expression vector pAcGFP1-C1 (Clontech) with pHluorin2 between the *Nhe*I and *Xho*I sites. This new vector was named pAcpHluorin2-C1. Next, human TGN46 was inserted in-frame C-terminal to pHluorin2 between the *Kpn*I and *Bam*HI sites of pAcpHluorin2-C1. To ensure proper targeting of $_{pH2}$TGN46, the signal sequence of TGN46 (i.e. first 21 amino acids) was inserted N-terminal to $_{pH2}$TGN46 by PCR mutagenesis using the *Nhe*I and

*Bam*HI restriction sites. All constructs were sequenced to confirm that no additional mutations were introduced during PCR. The temperature-sensitive variant (ts045) of VSVG glycoprotein tagged with GFP was kindly provided by Dr John Presley (McGill University).

### Cell culture and transfection

AP-1 cells (Chinese hamster ovary fibroblasts that lack PM NHE1) were grown to subconfluence in $\alpha$-MEM supplemented with 10% fetal bovine serum, penicillin (100 units/ml), streptomycin (100 µg/ml) and 25 mM $NaHCO_3$ (pH 7.4). Plasmid DNA was transiently transfected into AP-1 cells using Lipofectamine2000™ (Invitrogen) according to the manufacturer's recommended protocols. Cells were cultured in a humidified atmosphere of 5% $CO_2$ and 95% air at 37°C (unless otherwise indicated).

### Western blotting

For western blot analyses, AP-1 cells were grown in 3.5 or 10 cm dishes and transiently transfected with 2–5 µg of plasmid DNA encoding $SLC9A7_{HA}$ WT or L515F constructs [along with $VSVG_{GFP}$ (5 µg) in some experiments] according to the manufacturer's recommended procedures. Cell lysates were prepared and analysed as previously described (29).

### Endoglycosidase treatment

To assess the glycosylation status of SLC9A7, AP-1 cells were grown in 10 cm dishes and then transiently transfected with $SLC9A7_{HA}$ WT or L515F as described above. Thirty-six hours post-transfection, post-nuclear supernatants prepared and treated with Endo H (750 units, New England Biolabs, Mississauga, ON, Canada) or PNGase F according to the manufacturer's recommendations as previously described (29). Treated samples were then diluted with 2-fold concentrated SDS-PAGE sample buffer, incubated on a rocker for 30 min at room temperature, briefly centrifuged and analysed by SDS-PAGE and western blotting with a mouse monoclonal anti-HA antibody.

### Cell surface biotinylation

AP-1 cells transiently expressing $SLC9A7_{HA}$ WT or L515F were cultured in 10 cm dishes to sub-confluence, placed on ice and washed twice with ice-cold phosphate-buffered saline (PBS) containing 1 mM $MgCl_2$ and 0.1 mM $CaCl_2$, pH 8.0 phosphate-buffered saline containing calcium and magnesium (PBS-CM). Cells were then incubated at 4°C for 30 min with the membrane-impermeable reagent N-hydroxysulfosuccinimydyl-SS-biotin (0.5 mg/ml; ThermoScientific, Rockford, IL, USA), and the biotinylated PM protein were extracted with a NeutrAvidin® Agarose Resin slurry (Fisher Scientific, Whitby, ON, Canada) as previously described (29). The proteins in the total lysates and surface fractions were resolved by SDS-PAGE and analysed by western blotting.

### Measurement of SLC9A7 half-life

To determine the stability of $SLC9A7_{HA}$ WT and L515F proteins, AP-1 cells were grown in 3.5 cm dishes and transiently transfected with WT or L515F constructs. Twenty-four hours post-transfection, cells were treated with cycloheximide (150 µg/ml) to inhibit new protein synthesis in $\alpha$-MEM supplemented with 10% fetal bovine serum (FBS) and penicillin/streptomycin for up to 24 h. At specific time points, cells were lysed, protein concentrations were measured and equal quantities of protein (30 µg) were subjected to SDS-PAGE and immunoblotting with a mouse monoclonal anti-HA antibody and rabbit polyclonal αCANX (as a loading control). The intensities of the bands were quantified by densitometry of X-ray films exposed in the linear range and analysed using ImageJ software. Data were modelled to an exponential decay using a fit function (y = A1*exp(−x/t1) + y0).

### Fluorescence confocal microscopy

AP-1 cells were cultured overnight on fibronectin-coated 18 mm glass coverslips and transiently co-transfected with a fluorescent marker to label the TGN compartment ($TGN46_{EmGFP}$) and a monomeric ChFP-tagged SLC9A7 ($SLC9A7_{ChFP}$) WT or L515F (0.4 µg each). Cells were then fixed 24 h post transfection with 4% paraformaldehyde for 20 min at room temperature and mounted onto glass slides. A Zeiss LSM 780 confocal microscope, equipped with a photomultiplier tube (PMT) detector and a 63×/1.4 NA oil immersion objective lens, was used to obtain the images. These images were then prepared and presented using Zeiss ZEN and CorelDraw™ X6 software.

### Ratiometric measurement of intraluminal pH

AP-1 cells were grown overnight on FluoroDishes™ (World Precision Instruments, Inc.) coated with fibronectin/PBS (2 µg/ml, for 2–4 h at 37°C). Cells were transfected with 1 µg DNA/dish of $_{pH2}$WT, $_{pH2}$L515F or $_{pH2}$TGN46 using Lipofectamine2000 reagent according to the manufacturer's instructions. Twenty-four hours after transfection, cells were incubated for 3 h with 100 µg/ml cycloheximide in complete medium to block *de novo* protein synthesis and allow the newly synthesized constructs to exit the ER. During imaging, cells were maintained under physiological culture conditions in a microscope stage-top incubator (i.e. complete α-MEM media buffered with 22 mM $NaHCO_3$ and equilibrated with 5% $CO_2$ and 95% air at 37°C). Intraluminal pH was measured by single-cell FRIA (56), using a Zeiss LSM 780 confocal microscope, equipped with a PMT detector. Images were acquired with a 63×/1.4 NA oil immersion objective lens by sequential line scanning at 405 and 488 excitation wavelengths, with emission set at 500–550 for both channels. All cells were imaged in a heated chamber (37°C) at 3× zoom, while the laser power, resolution, speed of scanning, digital gain and offset, pinhole opening and line averaging were identical for both channels. Average intensities of fluorescent puncta (0.3–3 µm in diameter) were obtained for both the 405 and 488 channels using the MetaXpress software (Molecular Devices, Downingtown, PA, USA) and 488/405 ratios were calculated. Calibration curves of fluorescence as a function of intraluminal pH were performed *in situ* in AP-1 cells expressing $_{pH2}$WT or $_{pH2}$TGN46 by clamping the vesicular pH between 5.0 and 7.8 in $K^+$-rich medium (135 mM KCl, 10 mM NaCl, 20 mM HEPES (4-(2-hydroxyethyl)-1-piperazineethanesulfonic acid) or 20 mM MES (2-(N-morpholino) ethanesulfonic acid), 1 mM MgCl2, and 0.1 mM CaCl2) with 10 µm nigericin, 10 µm monensin, 0.4 µm bafilomycin and 20 µm carbonyl cyanide m-chlorophenyl hydrazone and recording the 488/405 fluorescence ratios, as described above. The calibration curves and Gaussian distributions of intraluminal pH values were plotted with OriginPro 8 software (OriginLab, Northampton, MA, USA).

### Statistical analyses

The data represent the mean ± the standard error of the mean (S.E.M.) and statistical analyses were performed using a two-sample Student's *t*-test or one-way analysis of variance (ANOVA). A minimum *P*-value of $<0.05$ was considered significant.

## Supplementary Material

Supplementary Material is available at *HMG* online.

## Acknowledgements

We are grateful for the services provided by McGill Life Sciences Advanced BioImaging Facility and Genome Québec for DNA sequencing, both platforms supported by funding from the Canadian Foundation for Innovation.

*Conflict of Interest statement*. The authors declare that they have no competing interests.

## Funding

Canadian Institutes of Health Research (MOP-111191, PJT-155976) and Faculty of Medicine (McGill University) to J.O.; the EU FP7 project GENCODYS (grant number 241995 to V.M.K.); and Channel 7 Children's Research Foundation support and Australian NHMRC grants (APP1041920 and APP1091593 to J.G.). W.K. is the recipient of a scholarship from the Government of Saudi Arabia.

## Author contributions

W.K. and A.I. performed molecular, biochemical and fluorescence imaging studies and data analyses; A.I. performed the ratiometric vesicular pH measurements; J.O. designed, supervised and coordinated different aspects of the *in vitro* experiments and data analyses; A.H., T.D.-B., L.C. and M.F. were clinicians involved with family AU; M.S., V.M.K., M.A.C., K.L.F. and J.G. performed the genetics analyses of family AU; B.M.K. was the clinician involved with family US; J.J. performed the genetics analyses of family US; W.K. and J.O. wrote the manuscript; all authors critically discussed results, revised and approved the manuscript.

## References

1. Aicardi, J. (1998) The etiology of developmental delay. *Semin. Pediatr. Neurol.*, **5**, 15–20.
2. Leonard, H. and Wen, X. (2002) The epidemiology of mental retardation: challenges and opportunities in the new millennium. *Ment. Retard. Dev. Disabil. Res. Rev.*, **8**, 117–134.
3. de Ligt, J., Willemsen, M.H., van Bon, B.W., Kleefstra, T., Yntema, H.G., Kroes, T., Vulto-van Silfhout, A.T., Koolen, D.A., de Vries, P., Gilissen, C. *et al.* (2012) Diagnostic exome sequencing in persons with severe intellectual disability. *N. Engl. J. Med.*, **367**, 1921–1929.
4. Gilissen, C., Hehir-Kwa, J.Y., Thung, D.T., van de Vorst, M., van Bon, B.W., Willemsen, M.H., Kwint, M., Janssen, I.M., Hoischen, A., Schenck, A. *et al.* (2014) Genome sequencing identifies major causes of severe intellectual disability. *Nature*, **511**, 344–347.
5. Harripaul, R., Vasli, N., Mikhailov, A., Rafiq, M.A., Mittal, K., Windpassinger, C., Sheikh, T.I., Noor, A., Mahmood, H., Downey, S. *et al.* (2017) Mapping autosomal recessive intellectual disability: combined microarray and exome sequencing identifies 26 novel candidate genes in 192 consanguineous families. *Mol. Psychiatry*, **23**, 973–984.
6. Vissers, L.E., Gilissen, C. and Veltman, J.A. (2016) Genetic studies in intellectual disability and related disorders. *Nat. Rev. Genet.*, **17**, 9–18.
7. Tarpey, P.S., Smith, R., Pleasance, E., Whibley, A., Edkins, S., Hardy, C., O'Meara, S., Latimer, C., Dicks, E., Menzies, A. *et al.* (2009) A systematic, large-scale resequencing screen of X-chromosome coding exons in mental retardation. *Nat. Genet.*, **41**, 535–543.
8. Gécz, J., Shoubridge, C. and Corbett, M. (2009) The genetic landscape of intellectual disability arising from chromosome X. *Trends Genet.*, **25**, 308–316.
9. Ropers, H.H. (2010) Genetics of early onset cognitive impairment. *Annu. Rev. Genomics Hum. Genet.*, **11**, 161–187.
10. Lubs, H.A., Stevenson, R.E. and Schwartz, C.E. (2012) Fragile X and X-linked intellectual disability: four decades of discovery. *Am. J. Hum. Genet.*, **90**, 579–590.
11. Hu, H., Haas, S.A., Chelly, J., Van, E.H., Raynaud, M., de Brouwer, A.P., Weinert, S., Froyen, G., Frints, S.G., Laumonnier, F. *et al.* (2016) X-exome sequencing of 405 unresolved families identifies seven novel intellectual disability genes. *Mol. Psychiatry*, **21**, 133–148.
12. Chelly, J., Khelfaoui, M., Francis, F., Cherif, B. and Bienvenu, T. (2006) Genetics and pathophysiology of mental retardation. *Eur. J. Hum. Genet.*, **14**, 701–713.
13. van Bokhoven, H. and Kramer, J.M. (2010) Disruption of the epigenetic code: an emerging mechanism in mental retardation. *Neurobiol. Dis.*, **39**, 3–12.
14. Rafiq, M.A., Kuss, A.W., Puettmann, L., Noor, A., Ramiah, A., Ali, G., Hu, H., Kerio, N.A., Xiang, Y., Garshasbi, M. *et al.* (2011) Mutations in the alpha 1,2-mannosidase gene, MAN1B1, cause autosomal-recessive intellectual disability. *Am. J. Hum. Genet.*, **89**, 176–182.
15. van Karnebeek, C.D. and Stockler, S. (2012) Treatable inborn errors of metabolism causing intellectual disability: a systematic literature review. *Mol. Genet. Metab.*, **105**, 368–381.
16. Valenti, D., de Bari, L., De Filippis, B., Henrion-Caude, A. and Vacca, R.A. (2014) Mitochondrial dysfunction as a central actor in intellectual disability-related diseases: an overview of Down syndrome, autism, Fragile X and Rett syndrome. *Neurosci. Biobehav. Rev.*, **46** Pt 2, 202–217.
17. Khan, M.A., Khan, S., Windpassinger, C., Badar, M., Nawaz, Z. and Mohammad, R.M. (2016) The molecular genetics of autosomal recessive nonsyndromic intellectual disability: a mutational continuum and future recommendations. *Ann. Hum. Genet.*, **80**, 342–368.
18. Najmabadi, H., Hu, H., Garshasbi, M., Zemojtel, T., Abedini, S.S., Chen, W., Hosseini, M., Behjati, F., Haas, S., Jamali, P. *et al.* (2011) Deep sequencing reveals 50 novel genes for recessive cognitive disorders. *Nature*, **478**, 57–63.
19. Hu, H., Kahrizi, K., Musante, L., Fattahi, Z., Herwig, R., Hosseini, M., Oppitz, C., Abedini, S.S., Suckow, V., Larti, F. *et al.* (2018) Genetics of intellectual disability in consanguineous families. *Mol. Psychiatry*. doi:10.1038/s41380-017-0012-2.
20. Vaillend, C., Poirier, R. and Laroche, S. (2008) Genes, plasticity and mental retardation. *Behav. Brain Res.*, **192**, 88–105.
21. Humeau, Y., Gambino, F., Chelly, J. and Vitale, N. (2009) X-linked mental retardation: focus on synaptic function and plasticity. *J. Neurochem.*, **109**, 1–14.
22. Numata, M. and Orlowski, J. (2001) Molecular cloning and characterization of a novel $(Na^+,K^+)/H^+$ exchanger localized to the trans-Golgi network. *J. Biol. Chem.*, **276**, 17387–17394.
23. Morton, N.E. (1996) Logarithm of odds (lods) for linkage in complex inheritance. *Proc. Natl. Acad. Sci. USA*, **93**, 3471–3476.

24. Thiselton, D.L., McDowall, J., Brandau, O., Ramser, J., d'Esposito, F., Bhattacharya, S.S., Ross, M.T., Hardcastle, A.J. and Meindl, A. (2002) An integrated, functionally annotated gene map of the DXS8026-ELK1 interval on human Xp11.3-Xp11.23: potential hotspot for neurogenetic disorders. *Genomics*, **79**, 560–572.
25. Layer, R.M., Chiang, C., Quinlan, A.R. and Hall, I.M. (2014) LUMPY: a probabilistic framework for structural variant discovery. *Genome Biol.*, **15**, R84.
26. Philippakis, A.A., Azzariti, D.R., Beltran, S., Brookes, A.J., Brownstein, C.A., Brudno, M., Brunner, H.G., Buske, O.J., Carey, K., Doll, C. *et al.* (2015) The Matchmaker Exchange: a platform for rare disease gene discovery. *Hum. Mutat.*, **36**, 915–921.
27. Traynelis, J., Silk, M., Wang, Q., Berkovic, S.F., Liu, L., Ascher, D.B., Balding, D.J. and Petrovski, S. (2017) Optimizing genomic medicine in epilepsy through a gene-customized approach to missense variant interpretation. *Genome Res.*, **27**, 1715–1729.
28. Lek, M., Karczewski, K.J., Minikel, E.V., Samocha, K.E., Banks, E., Fennell, T., O'Donnell-Luria, A.H., Ware, J.S., Hill, A.J., Cummings, B.B. *et al.* (2016) Analysis of protein-coding genetic variation in 60,706 humans. *Nature*, **536**, 285–291.
29. Ilie, A., Gao, A.Y.L., Reid, J., Boucher, A., McEwan, C., Barriere, H., Lukacs, G.L., McKinney, R.A. and Orlowski, J. (2016) A Christianson syndrome-linked deletion mutation ($\Delta^{287}ES^{288}$) in SLC9A6 disrupts recycling endosomal function and elicits neurodegeneration and cell death. *Mol. Neurodegener.*, **11**, 1–28.
30. Fliegel, L., Haworth, R.S. and Dyck, J.R.B. (1993) Characterization of the placental brush border membrane $Na^+/H^+$ exchanger: identification of thiol-dependent transitions in apparent molecular size. *Biochem. J*, **289**, 101–107.
31. Fafournoux, P., Noël, J. and Pouysségur, J. (1994) Evidence that $Na^+/H^+$ exchanger isoforms NHE1 and NHE3 exist as stable dimers in membranes with a high degree of specificity for homodimers. *J. Biol. Chem*, **269**, 2589–2596.
32. Lin, P.J., Williams, W.P., Luu, Y., Molday, R.S., Orlowski, J. and Numata, M. (2005) Secretory carrier membrane proteins interact and regulate trafficking of the organellar ($Na^+$,$K^+$)/$H^+$ exchanger NHE7. *J. Cell Sci.*, **118**, 1885–1897.
33. Fukura, N., Ohgaki, R., Matsushita, M., Nakamura, N., Mitsui, K. and Kanazawa, H. (2010) A membrane-proximal region in the C-terminal tail of NHE7 is required for its distribution in the trans-Golgi network, distinct from NHE6 localization at endosomes. *J. Membr. Biol.*, **234**, 149–158.
34. Le Bivic, A., Real, F.X. and Rodriguez-Boulan, E. (1989) Vectorial targeting of apical and basolateral plasma membrane proteins in a human adenocarcinoma epithelial cell line. *Proc. Natl. Acad. Sci. U. S. A.*, **86**, 9313–9317.
35. Mellman, I. (1992) The importance of being acid: the role of acidification in intracellular membrane traffic. *J. Exp. Biol.*, **172**, 39–45.
36. Schoonderwoert, V.T., Holthuis, J.C., Tanaka, S., Tooze, S.A. and Martens, G.J. (2000) Inhibition of the vacuolar $H^+$-ATPase perturbs the transport, sorting, processing and release of regulated secretory proteins. *Eur. J. Biochem.*, **267**, 5646–5654.
37. Kim, J.H., Johannes, L., Goud, B., Antony, C., Lingwood, C.A., Daneman, R. and Grinstein, S. (1998) Noninvasive measurement of the pH of the endoplasmic reticulum at rest and during calcium release. *Proc. Natl. Acad. Sci. U. S. A.*, **95**, 2997–3002.
38. Wu, M.M., Llopis, J., Adams, S., McCaffery, J.M., Kulomaa, M.S., Machen, T.E., Moore, H.P. and Tsien, R.Y. (2000) Organelle pH studies using targeted avidin and fluorescein-biotin. *Chem. Biol.*, **7**, 197–209.
39. Kim, J.H., Lingwood, C.A., Williams, D.B., Furuya, W., Manolson, M.F. and Grinstein, S. (1996) Dynamic measurement of the pH of the Golgi complex in living cells using retrograde transport of the verotoxin receptor. *J. Cell Biol.*, **134**, 1387–1399.
40. Llopis, J., McCaffery, J.M., Miyawaki, A., Farquhar, M.G. and Tsien, R.Y. (1998) Measurement of cytosolic, mitochondrial, and Golgi pH in single living cells with green fluorescent proteins. *Proc. Natl. Acad. Sci. U. S. A.*, **95**, 6803–6808.
41. Seksek, O., Biwersi, J. and Verkman, A.S. (1995) Direct measurement of trans-Golgi pH in living cells and regulation by second messengers. *J. Biol. Chem.*, **270**, 4967–4970.
42. Demaurex, N., Furuya, W., D'Souza, S., Bonifacino, J.S. and Grinstein, S. (1998) Mechanism of acidification of the trans-Golgi network (TGN). In situ measurements of pH using retrieval of TGN38 and furin from the cell surface. *J. Biol. Chem.*, **273**, 2044–2051.
43. Miesenböck, G., De Angelis, D.A. and Rothman, J.E. (1998) Visualizing secretion and synaptic transmission with pH-sensitive green fluorescent proteins. *Nature*, **394**, 192–195.
44. Machen, T.E., Leigh, M.J., Taylor, C., Kimura, T., Asano, S. and Moore, H.P. (2003) pH of TGN and recycling endosomes of $H^+/K^+$-ATPase-transfected HEK-293 cells: implications for pH regulation in the secretory pathway. *Am. J. Physiol. Cell Physiol.*, **285**, C205–C214.
45. Wu, M.M., Grabe, M., Adams, S., Tsien, R.Y., Moore, H.P. and Machen, T.E. (2001) Mechanisms of pH regulation in the regulated secretory pathway. *J. Biol. Chem.*, **276**, 33027–33035.
46. Glickman, J., Croen, K., Kelly, S. and Al-Awqati, Q. (1983) Golgi membranes contain an electrogenic $H^+$ pump in parallel to a chloride conductance. *J. Cell Biol.*, **97**, 1303–1308.
47. Marshansky, V. and Futai, M. (2008) The V-type $H^+$-ATPase in vesicular trafficking: targeting, regulation and function. *Curr. Opin. Cell Biol.*, **20**, 415–426.
48. Nagasawa, M., Kanzaki, M., Iino, Y., Morishita, Y. and Kojima, I. (2001) Identification of a novel chloride channel expressed in the endoplasmic reticulum, golgi apparatus, and nucleus. *J. Biol. Chem.*, **276**, 20413–20418.
49. Nordeen, M.H., Jones, S.M., Howell, K.E. and Caldwell, J.H. (2000) GOLAC: an endogenous anion channel of the Golgi complex. *Biophys. J.*, **78**, 2918–2928.
50. Thompson, R.J., Nordeen, M.H., Howell, K.E. and Caldwell, J.H. (2002) A large-conductance anion channel of the Golgi complex. *Biophys. J.*, **83**, 278–289.
51. Maeda, Y., Ide, T., Koike, M., Uchiyama, Y. and Kinoshita, T. (2008) GPHR is a novel anion channel critical for acidification and functions of the Golgi apparatus. *Nat. Cell Biol.*, **10**, 1135–1145.
52. Schapiro, F.B. and Grinstein, S. (2000) Determinants of the pH of the Golgi complex. *J. Biol. Chem.*, **275**, 21025–21032.
53. Nakamura, N., Tanaka, S., Teko, Y., Mitsui, K. and Kanazawa, H. (2005) Four $Na^+/H^+$ exchanger isoforms are distributed to Golgi and post-Golgi compartments and are involved in organelle pH regulation. *J. Biol. Chem.*, **280**, 1561–1572.
54. Lawrence, S.P., Bright, N.A., Luzio, J.P. and Bowers, K. (2010) The sodium/proton exchanger NHE8 regulates late endosomal morphology and function. *Mol. Biol. Cell*, **21**, 3540–3551.

55. Mahon, M.J. (2011) pHluorin2: an enhanced, ratiometric, pH-sensitive green florescent protein. *Adv. Biosci. Biotechnol.*, **2**, 132–137.
56. Barrière, H., Apaja, P., Okiyoneda, T. and Lukacs, G.L. (2011) Endocytic sorting of CFTR variants monitored by single-cell fluorescence ratiometric image analysis (FRIA) in living cells. *Methods Mol. Biol.*, **741**, 301–317.
57. Kellokumpu, S., Sormunen, R. and Kellokumpu, I. (2002) Abnormal glycosylation and altered Golgi structure in colorectal cancer: dependence on intra-Golgi pH. *FEBS Lett.*, **516**, 217–224.
58. Maeda, Y. and Kinoshita, T. (2010) The acidic environment of the Golgi is critical for glycosylation and transport. *Methods Enzymol.*, **480**, 495–510.
59. Huang, C. and Chang, A. (2011) pH-dependent cargo sorting from the Golgi. *J. Biol. Chem.*, **286**, 10058–10065.
60. Rivinoja, A., Pujol, F.M., Hassinen, A. and Kellokumpu, S. (2012) Golgi pH, its regulation and roles in human disease. *Ann. Med.*, **44**, 542–554.
61. de Silva, A.M., Balch, W.E. and Helenius, A. (1990) Quality control in the endoplasmic reticulum: folding and misfolding of vesicular stomatitis virus G protein in cells and in vitro. *J. Cell Biol.*, **111**, 857–866.
62. Presley, J.F., Cole, N.B., Schroer, T.A., Hirschberg, K., Zaal, K.J. and Lippincott-Schwartz, J. (1997) ER-to-Golgi transport visualized in living cells. *Nature*, **389**, 81–85.
63. Babovic-Vuksanovic, D. and O'Brien, J.F. (2007) Laboratory diagnosis of congenital disorders of glycosylation type I by analysis of transferrin glycoforms. *Mol. Diagn. Ther.*, **11**, 303–311.
64. Van Scherpenzeel, M., Willems, E. and Lefeber, D.J. (2016) Clinical diagnostics and therapy monitoring in the congenital disorders of glycosylation. *Glycoconj. J.*, **33**, 345–358.
65. Scott, K., Gadomski, T., Kozicz, T. and Morava, E. (2014) Congenital disorders of glycosylation: new defects and still counting. *J. Inherit. Metab. Dis.*, **37**, 609–617.
66. Hennet, T. and Cabalzar, J. (2015) Congenital disorders of glycosylation: a concise chart of glycocalyx dysfunction. *Trends Biochem. Sci.*, **40**, 377–384.
67. Wada, Y. (2016) Mass spectrometry of transferrin glycoforms to detect congenital disorders of glycosylation: site-specific profiles and pitfalls. *Proteomics*, **16**, 3105–3110.
68. Guissart, C., Li, X., Leheup, B., Drouot, N., Montaut-Verient, B., Raffo, E., Jonveaux, P., Roux, A.F., Claustres, M., Fliegel, L. *et al.* (2015) Mutation of SLC9A1, encoding the major $Na^+/H^+$ exchanger, causes ataxia-deafness Lichtenstein–Knorr syndrome. *Hum. Mol. Genet.*, **24**, 463–470.
69. Gilfillan, G.D., Selmer, K.K., Roxrud, I., Smith, R., Kyllerman, M., Eiklid, K., Kroken, M., Mattingsdal, M., Egeland, T., Stenmark, H. *et al.* (2008) SLC9A6 mutations cause X-linked mental retardation, microcephaly, epilepsy, and ataxia, a phenotype mimicking Angelman syndrome. *Am. J. Hum. Genet.*, **82**, 1003–1010.
70. Pescosolido, M.F., Stein, D.M., Schmidt, M., Moufawad El, A.C., Sabbagh, M., Rogg, J.M., Tantravahi, U., McLean, R.L., Liu, J.S., Poduri, A. *et al.* (2014) Genetic and phenotypic diversity of NHE6 mutations in Christianson syndrome. *Ann. Neurol.*, **76**, 581–593.
71. Morrow, E.M., Yoo, S.Y., Flavell, S.W., Kim, T.K., Lin, Y., Hill, R.S., Mukaddes, N.M., Balkhy, S., Gascon, G., Hashmi, A. *et al.* (2008) Identifying autism loci and genes by tracing recent shared ancestry. *Science*, **321**, 218–223.
72. Schwede, M., Garbett, K., Mirnics, K., Geschwind, D.H. and Morrow, E.M. (2013) Genes for endosomal NHE6 and NHE9 are misregulated in autism brains. *Mol. Psychiatry*, **19**, 277–279.
73. de Silva, M.G., Elliott, K., Dahl, H.H., Fitzpatrick, E., Wilcox, S., Delatycki, M., Williamson, R., Efron, D., Lynch, M. and Forrest, S. (2003) Disruption of a novel member of a sodium/hydrogen exchanger family and DOCK3 is associated with an attention deficit hyperactivity disorder-like phenotype. *J. Med. Genet.*, **40**, 733–740.
74. Lasky-Su, J., Neale, B.M., Franke, B., Anney, R.J., Zhou, K., Maller, J.B., Vasquez, A.A., Chen, W., Asherson, P., Buitelaar, J. *et al.* (2008) Genome-wide association scan of quantitative traits for attention deficit hyperactivity disorder identifies novel associations and confirms candidate gene associations. *Am. J. Med. Genet. B Neuropsychiatr. Genet.*, **147B**, 1345–1354.
75. Markunas, C.A., Quinn, K.S., Collins, A.L., Garrett, M.E., Lachiewicz, A.M., Sommer, J.L., Morrissey-Kane, E., Kollins, S.H., Anastopoulos, A.D. and Ashley-Koch, A.E. (2010) Genetic variants in SLC9A9 are associated with measures of attention-deficit/hyperactivity disorder symptoms in families. *Psychiatr. Genet.*, **20**, 73–81.
76. Ilie, A., Weinstein, E., Boucher, A., McKinney, R.A. and Orlowski, J. (2014) Impaired posttranslational processing and trafficking of an endosomal $Na^+/H^+$ exchanger NHE6 mutant ($\Delta^{370}WST^{372}$) associated with X-linked intellectual disability and autism. *Neurochem. Int.*, **73**, 192–203.
77. Rajasekaran, A.K., Humphrey, J.S., Wagner, M., Miesenböck, G., Le Bivic, A., Bonifacino, J.S. and Rodriguez-Boulan, E. (1994) TGN38 recycles basolaterally in polarized Madin-Darby canine kidney cells. *Mol. Biol. Cell*, **5**, 1093–1103.
78. Roquemore, E.P. and Banting, G. (1998) Efficient trafficking of TGN38 from the endosome to the trans-Golgi network requires a free hydroxyl group at position 331 in the cytosolic domain. *Mol. Biol. Cell*, **9**, 2125–2144.
79. Takahashi, S., Nakagawa, T., Banno, T., Watanabe, T., Murakami, K. and Nakayama, K. (1995) Localization of furin to the trans-Golgi network and recycling from the cell surface involves Ser and Tyr residues within the cytoplasmic domain. *J. Biol. Chem.*, **270**, 28397–28401.
80. Schäfer, W., Stroh, A., Berghöfer, S., Seiler, J., Vey, M., Kruse, M.L., Kern, H.F., Klenk, H.D. and Garten, W. (1995) Two independent targeting signals in the cytoplasmic domain determine trans-Golgi network localization and endosomal trafficking of the proprotein convertase furin. *EMBO J.*, **14**, 2424–2435.
81. Voorhees, P., Deignan, E., van Donselaar, E., Humphrey, J., Marks, M.S., Peters, P.J. and Bonifacino, J.S. (1995) An acidic sequence within the cytoplasmic domain of furin functions as a determinant of trans-Golgi network localization and internalization from the cell surface. *EMBO J.*, **14**, 4961–4975.
82. Delphin, N., Hanein, S., Taie, L.F., Zanlonghi, X., Bonneau, D., Moisan, J.P., Boyle, C., Nitschke, P., Pruvost, S., Bonnefont, J.P. *et al.* (2012) Intellectual disability associated with retinal dystrophy in the Xp11.3 deletion syndrome: ZNF674 on trial. Guilty or innocent? *Eur. J. Hum. Genet.*, **20**, 352–356.
83. Axelsson, M.A., Karlsson, N.G., Steel, D.M., Ouwendijk, J., Nilsson, T. and Hansson, G.C. (2001) Neutralization of pH in the Golgi apparatus causes redistribution of glycosyltransferases and changes in the O-glycosylation of mucins. *Glycobiology*, **11**, 633–644.

84. Hassinen, A., Pujol, F.M., Kokkonen, N., Pieters, C., Kihlström, M., Korhonen, K. and Kellokumpu, S. (2011) Functional organization of Golgi N- and O-glycosylation pathways involves pH-dependent complex formation that is impaired in cancer cells. *J. Biol. Chem.*, **286**, 38329–38340.
85. Rivinoja, A., Hassinen, A., Kokkonen, N., Kauppila, A. and Kellokumpu, S. (2009) Elevated Golgi pH impairs terminal N-glycosylation by inducing mislocalization of Golgi glycosyltransferases. *J. Cell Physiol.*, **220**, 144–154.
86. Ledger, P.W., Nishimoto, S.K., Hayashi, S. and Tanzer, M.L. (1983) Abnormal glycosylation of human fibronectin secreted in the presence of monensin. *J. Biol. Chem.*, **258**, 547–554.
87. Thorens, B. and Vassalli, P. (1986) Chloroquine and ammonium chloride prevent terminal glycosylation of immunoglobulins in plasma cells without affecting secretion. *Nature*, **321**, 618–620.
88. Mollenhauer, H.H., Morré, D.J. and Rowe, L.D. (1990) Alteration of intracellular traffic by monensin; mechanism, specificity and relationship to toxicity. *Biochim. Biophys. Acta*, **1031**, 225–246.
89. Hirata, Y., Shimokawa, N., Oh-hashi, K., Yu, Z.X. and Kiuchi, K. (2010) Acidification of the Golgi apparatus is indispensable for maturation but not for cell surface delivery of Ret. *J. Neurochem.*, **115**, 606–613.
90. Kornak, U., Reynders, E., Dimopoulou, A., van, R.J., Fischer, B., Rajab, A., Budde, B., Nürnberg, P., Foulquier, F., Lefeber, D. *et al.* (2008) Impaired glycosylation and cutis laxa caused by mutations in the vesicular $H^+$-ATPase subunit ATP6V0A2. *Nat. Genet.*, **40**, 32–34.
91. Van Damme, T., Gardeitchik, T., Mohamed, M., Guerrero-Castillo, S., Freisinger, P., Guillemyn, B., Kariminejad, A., Dalloyaux, D., van Kraaij, S., Lefeber, D.J. *et al.* (2017) Mutations in ATP6V1E1 or ATP6V1A cause autosomal-recessive cutis laxa. *Am. J. Hum. Genet.*, **100**, 216–227.
92. Péanne, R., de Lonlay, P., Foulquier, F., Kornak, U., Lefeber, D.J., Morava, E., Pérez, B., Seta, N., Thiel, C., Van Schaftingen, E. *et al.* (2018) Congenital disorders of glycosylation (CDG): quo vadis? *Eur. J. Med. Genet.*, **61**, 643–663.
93. Helenius, A. and Aebi, M. (2001) Intracellular functions of N-linked glycans. *Science*, **291**, 2364–2369.
94. Haltiwanger, R.S. and Lowe, J.B. (2004) Role of glycosylation in development. *Annu. Rev. Biochem.*, **73**, 491–537.
95. Ohtsubo, K. and Marth, J.D. (2006) Glycosylation in cellular mechanisms of health and disease. *Cell*, **126**, 855–867.
96. Bieberich, E. (2014) Synthesis, processing, and function of N-glycans in N-glycoproteins. *Adv. Neurobiol.*, **9**, 47–70.
97. Patterson, M.C. (2005) Metabolic mimics: the disorders of N-linked glycosylation. *Semin. Pediatr. Neurol.*, **12**, 144–151.
98. Haliloğlu, G. and Topaloğlu, H. (2004) Glycosylation defects in muscular dystrophies. *Curr. Opin. Neurol.*, **17**, 521–527.
99. Maverakis, E., Kim, K., Shimoda, M., Gershwin, M.E., Patel, F., Wilken, R., Raychaudhuri, S., Ruhaak, L.R. and Lebrilla, C.B. (2015) Glycans in the immune system and the altered glycan theory of autoimmunity: a critical review. *J. Autoimmun.*, **57**, 1–13.
100. Epp, A., Sullivan, K.C., Herr, A.B. and Strait, R.T. (2016) Immunoglobulin glycosylation effects in allergy and immunity. *Curr. Allergy Asthma Rep.*, **16**, 79.
101. Freeze, H.H., Eklund, E.A., Ng, B.G. and Patterson, M.C. (2015) Neurological aspects of human glycosylation disorders. *Annu. Rev. Neurosci.*, **38**, 105–125.
102. Angata, K., Huckaby, V., Ranscht, B., Terskikh, A., Marth, J.D. and Fukuda, M. (2007) Polysialic acid-directed migration and differentiation of neural precursors are essential for mouse brain development. *Mol. Cell. Biol.*, **27**, 6659–6668.
103. Burgess, A., Wainwright, S.R., Shihabuddin, L.S., Rutishauser, U., Seki, T. and Aubert, I. (2008) Polysialic acid regulates the clustering, migration, and neuronal differentiation of progenitor cells in the adult hippocampus. *Dev. Neurobiol.*, **68**, 1580–1590.
104. Rutishauser, U. and Landmesser, L. (1996) Polysialic acid in the vertebrate nervous system: a promoter of plasticity in cell–cell interactions. *Trends Neurosci.*, **19**, 422–427.
105. Kleene, R. and Schachner, M. (2004) Glycans and neural cell interactions. *Nat. Rev. Neurosci.*, **5**, 195–208.
106. Dityatev, A., Dityateva, G., Sytnyk, V., Delling, M., Toni, N., Nikonenko, I., Muller, D. and Schachner, M. (2004) Polysialylated neural cell adhesion molecule promotes remodeling and formation of hippocampal synapses. *J. Neurosci.*, **24**, 9372–9382.
107. Chang, W.P. and Südhof, T.C. (2009) SV2 renders primed synaptic vesicles competent for $Ca^{2+}$-induced exocytosis. *J. Neurosci.*, **29**, 883–897.
108. Kwon, S.E. and Chapman, E.R. (2012) Glycosylation is dispensable for sorting of synaptotagmin 1 but is critical for targeting of SV2 and synaptophysin to recycling synaptic vesicles. *J. Biol. Chem.*, **287**, 35658–35668.
109. Tate, C.G. and Blakely, R.D. (1994) The effect of N-linked glycosylation on activity of the $Na^+$- and $Cl^-$-dependent serotonin transporter expressed using recombinant baculovirus in insect cells. *J. Biol. Chem.*, **269**, 26303–26310.
110. Melikian, H.E., Ramamoorthy, S., Tate, C.G. and Blakely, R.D. (1996) Inability to N-glycosylate the human norepinephrine transporter reduces protein stability, surface trafficking, and transport activity but not ligand recognition. *Mol. Pharmacol.*, **50**, 266–276.
111. Olivares, L., Aragón, C., Giménez, C. and Zafra, F. (1995) The role of N-glycosylation in the targeting and activity of the GLYT1 glycine transporter. *J. Biol. Chem.*, **270**, 9437–9442.
112. Martinez-Maza, R., Poyatos, I., López-Corcuera, B., Núñez, E., Giménez, C., Zafra, F. and Aragón, C. (2001) The role of N-glycosylation in transport to the plasma membrane and sorting of the neuronal glycine transporter GLYT2. *J. Biol. Chem.*, **276**, 2168–2173.
113. Li, L.B., Chen, N., Ramamoorthy, S., Chi, L., Cui, X.N., Wang, L.C. and Reith, M.E. (2004) The role of N-glycosylation in function and surface trafficking of the human dopamine transporter. *J. Biol. Chem.*, **279**, 21012–21020.
114. Cai, G., Salonikidis, P.S., Fei, J., Schwarz, W., Schülein, R., Reutter, W. and Fan, H. (2005) The role of N-glycosylation in the stability, trafficking and GABA-uptake of GABA-transporter 1. Terminal N-glycans facilitate efficient GABA-uptake activity of the GABA transporter. *FEBS J.*, **272**, 1625–1638.
115. Sutachan, J.J., Watanabe, I., Zhu, J., Gottschalk, A., Recio-Pinto, E. and Thornhill, W.B. (2005) Effects of Kv1.1 channel glycosylation on C-type inactivation and simulated action potentials. *Brain Res.*, **1058**, 30–43.
116. Zona, C., Eusebi, F. and Miledi, R. (1990) Glycosylation is required for maintenance of functional voltage-activated channels in growing neocortical neurons of the rat. *Proc. R. Soc. Lond. B Biol. Sci.*, **239**, 119–127.
117. Johnson, D., Montpetit, M.L., Stocker, P.J. and Bennett, E.S. (2004) The sialic acid component of the $\beta$1 subunit modu-

lates voltage-gated sodium channel function. *J. Biol. Chem.*, **279**, 44303–44310.
118. Ednie, A.R., Harper, J.M. and Bennett, E.S. (2015) Sialic acids attached to N- and O-glycans within the Nav1.4 D1S5-S6 linker contribute to channel gating. *Biochim. Biophys. Acta*, **1850**, 307–317.
119. Weiss, N., Black, S.A., Bladen, C., Chen, L. and Zamponi, G.W. (2013) Surface expression and function of Cav3.2 T-type calcium channels are controlled by asparagine-linked glycosylation. *Pflugers Arch.*, **465**, 1159–1170.
120. Scott, H. and Panin, V.M. (2014) The role of protein N-glycosylation in neural transmission. *Glycobiology*, **24**, 407–417.
121. Baycin-Hizal, D., Gottschalk, A., Jacobson, E., Mai, S., Wolozny, D., Zhang, H., Krag, S.S. and Betenbaugh, M.J. (2014) Physiologic and pathophysiologic consequences of altered sialylation and glycosylation on ion channel function. *Biochem. Biophys. Res. Commun.*, **453**, 243–253.
122. Matthies, H.,J., Kretlow, J., Matthies, H., Smalla, K.H., Staak, S. and Krug, M. (1999) Glycosylation of proteins during a critical time window is necessary for the maintenance of long-term potentiation in the hippocampal CA1 region. *Neuroscience*, **91**, 175–183.
123. Inaba, H., Kai, D. and Kida, S. (2016) N-glycosylation in the hippocampus is required for the consolidation and reconsolidation of contextual fear memory. *Neurobiol. Learn. Mem.*, **135**, 57–65.
124. Feliciangeli, S.F., Thomas, L., Scott, G.K., Subbian, E., Hung, C.H., Molloy, S.S., Jean, F., Shinde, U. and Thomas, G. (2006) Identification of a pH sensor in the furin propeptide that regulates enzyme activation. *J. Biol. Chem.*, **281**, 16108–16116.
125. Rockwell, N.C. and Fuller, R.S. (2002) Specific modulation of Kex2/furin family proteases by potassium. *J. Biol. Chem.*, **277**, 17531–17537.
126. Shaw, M., Yap, T.Y., Henden, L., Bahlo, M., Gardner, A., Kalscheuer, V.M., Haan, E., Christie, L., Hackett, A. and Gecz, J. (2015) Identical by descent L1CAM mutation in two apparently unrelated families with intellectual disability without L1 syndrome. *Eur. J. Med. Genet.*, **58**, 364–368.
127. Retterer, K., Juusola, J., Cho, M.T., Vitazka, P., Millan, F., Gibellini, F., Vertino-Bell, A., Smaoui, N., Neidich, J., Monaghan, K.G. *et al.* (2016) Clinical application of whole-exome sequencing across clinical indications. *Genet. Med.*, **18**, 696–704.